

**DORSAL CONVERGENCE OF GASTRULA CELLS REQUIRES A VANGL2
AND ADHESION PROTEIN-DEPENDENT CHANGE IN PROTRUSIVE
ACTIVITY**

By

Dianna J. Prince

A DISSERTATION

Submitted to

Middle Tennessee State University
Spring 2020

In partial fulfillment of the degree requirements
for the degree of

Doctorate of Philosophy in Molecular Biosciences

Dissertation Committee:
Dr. Jason R. Jessen, Chair
Dr. Christopher Herlihy
Dr. David Nelson
Dr. Matthew Elrod Erickson
Dr. Kevin Bicker

ACKNOWLEDGMENTS

I acknowledge the support and mentorship provided by my principal investigator, Jason R. Jessen. I acknowledge the graduate research assistantship I received during my tenure in the Jessen lab.

I acknowledge the support received from my lab mates: Anna Mooney Love and Anna Parnell.

I acknowledge technical support and guidance from Tammy Jessen.

I acknowledge the guidance provided by my dissertation committee Christopher Herlihy, David Nelson, Matthew Elrod Erickson, and Kevin Bicker.

I would like to thank my parents for supporting me throughout my academic career and enabling me to continue my education.

I would like to thank my son, Brody, for providing my inspiration while I strove to be an inspiration for him.

FUNDING

The studies detailed in this dissertation were funded by a grant from the National Institutes of Health (GM102356 to J.R.J.). Certain equipment items used to conduct this research were provided by Middle Tennessee State University. I acknowledge support from the Molecular Biosciences Ph.D. program and the Department of Biology.

ABSTRACT

During zebrafish gastrulation, planar cell polarity (PCP) describes the elongation and mediolateral alignment of cells parallel to their path of dorsal migration. The PCP pathway consists of a core group of proteins that includes VANGL planar cell polarity protein 2 (*Vangl2*) and a non-canonical Wnt/Glypican4 signaling pathway. Loss of function of a core PCP protein produces an embryo with a severe convergence and extension (C&E) phenotype characterized by a shortened and broadened dorsal axis. From mid- to late gastrulation mesodermal cells undergo a key transitional period. At 80% epiboly (mid-gastrulation) mesodermal cells exhibit rounder cell shapes, limited cell contacts, and indirect migration trajectories. By late gastrulation mesodermal cells elongate, pack together, and align into files as they engage in directed migration. The goal of this study was to gain understanding of this transition to polarized cell behaviors by examining the relationship between protrusion formation and the establishment of PCP and directed migration towards the dorsal axis. We found wild-type cells exhibit a reduction in the number of bleb protrusions formed between mid- and late gastrulation accompanied by a *Vangl2* regulated increase in filopodia. Increased bleb protrusions by *Ezrinb* knockdown disrupts PCP and directed migration. Additionally, we show that *Vangl2*, fibronectin, and N-cadherin are required for the suppression of blebbing at late gastrulation. *Vangl2* likely regulates blebbing by regulating *Ezrinb* protein levels, and increased *Ezrinb* activation in *vangl2* mutant embryos rescues the mediolateral cell alignment and directness defects of mesodermal cells. Lastly, transplantation experiments *vangl2* functions cell-autonomously to regulate protrusion formation while *fibronectin* is required non-autonomously.

Table of Contents

Chapter 1: Introduction

1.1 CELL MOVEMENTS DURING ZEBRAFISH GASTRULATION	3
<i>1.1.1 Epiboly</i>	<i>5</i>
<i>1.1.2 Internalization</i>	<i>5</i>
<i>1.1.3 Convergence and Extension.....</i>	<i>6</i>
1.2 PLANAR CELL POLARITY	7
1.3 SIGNIFICANCE OF PCP STUDIES	11
1.4 MEMBRANE PROTRUSIONS PRODUCED BY ZEBRAFISH GASTRULA CELLS.....	11
1.5 ADHESIVE PROTEINS- FIBRONECTIN AND CDH2	15
1.6 DISSERTATION GOAL	21

Chapter 2: Vangl2 is Required for Polarization of Filopodia at Late Gastrulation

2.1 INTRODUCTION	23
2.2 RESULTS.....	24
2.3 CONCLUSION.....	29

Chapter 3: Mesodermal Cells Exhibit Increased Bleb Protrusions at Mid-Gastrulation

3.1 INTRODUCTION	31
3.2 RESULTS.....	32
3.3 CONCLUSION.....	40

Chapter 4: Manipulation of Bleb Protrusive Activity at Mid- and Late Gastrulation

4.1 INTRODUCTION	42
4.2 RESULTS.....	43
4.3 CONCLUSION.....	52

Chapter 5: Role of Adhesive Proteins for Bleb Suppression at Late Gastrulation

5.1 INTRODUCTION	53
5.2 RESULTS.....	54
5.3 CONCLUSION.....	65

<i>Chapter 6: Vangl2 is Required for Bleb Suppression at Late Gastrulation and Functions Cell-Autonomously to Regulate Protrusions</i>	
6.1 INTRODUCTION	66
6.2 RESULTS	68
6.3 CONCLUSION	80
<i>Chapter 7: Discussion</i>	81
<i>Chapter 8: Materials and Methods</i>	
8.1 ZEBRAFISH HUSBANDRY AND GENETIC STRAINS	87
8.2 EMBRYO MICROINJECTION, MORPHOLINOS, AND SYNTHETIC MRNA	87
8.3 WHOLE-MOUNT <i>IN SITU</i> HYBRIDIZATION	88
8.4 WESTERN BLOT	89
8.5 IMMUNOFLUORESCENCE	90
8.6 DIC AND CONFOCAL IMAGING	90
8.7 QUANTITATION OF PCP, DIRECTED MIGRATION AND MEMBRANE PROTRUSIONS	91
8.8 CELL TRANSPLANTATION	92
8.9 STATISTICS	93
<i>Chapter 9: Bibliography</i>	93

Table of Figures

Figure 1. PCP in the fly wing epithelium	2
Figure 2. Cell movements during zebrafish gastrulation	4
Figure 3. Zebrafish PCP mutant phenotypes	9
Figure 4. Vertebrate PCP signaling pathway	10
Figure 5. Protrusion types formed during zebrafish gastrulation	13
Figure 6. Structure of classical cadherins	17
Figure 7. Structure of fibronectin	20
Figure 8. Greater filopodia production at late gastrulation	26
Figure 9. Vangl2 is needed for polarization of filopodia at late gastrulation	28
Figure 10. Bleb protrusion imaging by DIC and confocal microscopy	34
Figure 11. Increased bleb protrusions at mid-gastrulation	35
Figure 12. Mesendodermal cells produce highly polarized blebs in run phases	37
Figure 13. Increased activated Ezrinb at late gastrulation	39
Figure 14. Ezrinb morphants display a C&E phenotype	44
Figure 15. Blebbing at late gastrulation inhibits PCP	46
Figure 16. Ezrinb is required for directed migration	48
Figure 17. Western blot showing Ezrinb knockdown	50
Figure 18. ezrinb morphant embryos have mediolaterally broadened mesoderm	51
Figure 19. Cdh2 cell surface expression increases from mid- to late gastrulation	55
Figure 20. Fibronectin and Cdh2 facilitate proper PCP	57
Figure 21. Fibronectin and Cdh2 are required for proper bleb protrusive activity	59
Figure 22. Fibronectin and Cdh2 support directed migration	61
Figure 23. Western blot showing Cdh2 knockdown	63
Figure 24. Homozygous <i>cdh2^{tm101/tm101}</i> mutant embryos phenocopy <i>cdh2</i> morphants	64
Figure 25. PCP phenotype of <i>vangl2</i> mutant mesodermal cells	69
Figure 26. Loss of <i>Vangl2</i> causes greater blebbing in mesodermal cells	71
Figure 27. Inhibition of blebbing in <i>vangl2</i> mutants increases directed migration	73
Figure 28. <i>vangl2</i> acts cell-autonomously to regulate bleb protrusions	75
Figure 29. <i>vangl2</i> acts cell-autonomously to regulate filopodia protrusions	78
Figure 30. Ezrinb protein expression in <i>vangl2</i> mutant embryos	79

Table of Abbreviations

Cdh2	Cadherin2
DIC	Differential interference contrast
ECM	Extracellular matrix
Ezrb	Ezrinb
Fn	Fibronectin
LWR	Length-width ratio
memGFP	Membrane-targeted green fluorescent protein
memRFP	Membrane-targeted red fluorescent protein
MLA	Mediolateral alignment
MMP	Matrix metalloproteinase
MO	Morpholino
PCP	Planar cell polarity
Vangl2	VANGL planar cell polarity protein 2
WT	Wild type
Ypc/tb	Yolk-plug closure/tailbud

CHAPTER ONE. Introduction

Initially discovered in the wing epithelium of *Drosophila melanogaster*, planar cell polarity (PCP) was defined as the polarity of cells/cell structures within the plane of a tissue (opposite of apicobasal polarity). Six core PCP proteins were identified from studies in the fly: Frizzled, Dishevelled, Diego, Van Gogh, Prickle, and Flamingo. These core proteins were found to be distributed asymmetrically shortly before trichome/wing hair formation (Goodrich and Strutt, 2011). Each cell of the fly wing produces a single, actin-rich, distally-oriented trichome. Loss of function of a core PCP protein results in the loss of uniform trichome orientation (Goodrich and Strutt, 2011). Hallmarks of PCP in the fly wing include asymmetric protein localization and effects on actin cytoskeleton (Figure 1).

Contrary to the static structure of the fly wing epithelium, PCP is also implicated in collective groups of migrating cells such as zebrafish gastrula cell migration. During *Danio rerio* (zebrafish) gastrulation, convergence and extension (C&E) cell movements contribute to the development of the unstructured embryo into a gastrula with a distinct dorsal/ventral axis. C&E underlies the narrowing and lengthening of the body axis. These cell movements are dependent on the PCP signaling pathway. Proper function of PCP proteins is also necessary for ciliogenesis in the lung and brain, neural tube closure, and other morphogenetic processes (Wallingford and Mitchell, 2011). It is important to note PCP not only refers to the PCP signaling pathway and its core set of proteins but also the planar polarity observed in cells.

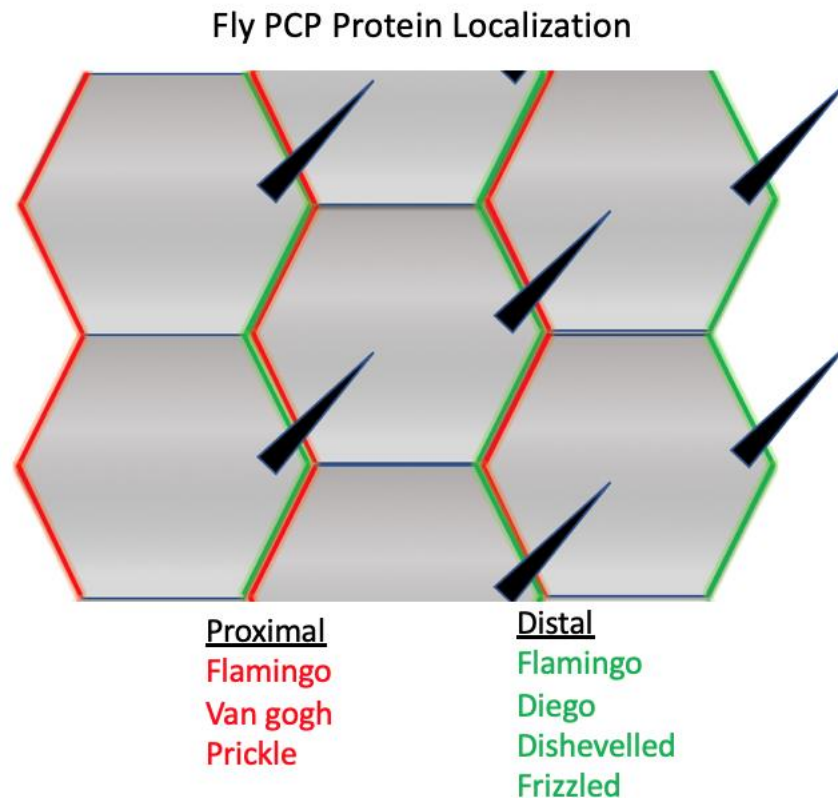


Figure 1. PCP in the fly wing epithelium: Core PCP protein localization and trichome orientation in epithelial cells of the fly wing. Wild-type wing epithelial cells show asymmetric localization of core PCP proteins. Green lines represent the localization of Flamingo, Diego, Dishevelled, and Frizzled at the distal edge of the cell, and red lines represent localization of Flamingo, Van gogh, and Prickle at the proximal edge of the cell.

1.1 Cell Movements During Gastrulation

Multiple gastrulation cell movements are involved during the creation of an embryo with a distinct anterior and posterior body axis such as epiboly, internalization, and C&E (Solnica-Krezel and Sepich, 2012). These movements do not occur sequentially, but rather concurrently over the course of gastrulation. Beginning at approximately 4 hours post-fertilization, the blastoderm thins and spreads to cover the yolk during epiboly. Once reaching 55% epiboly, gastrulation commences with the onset of internalization (Warga and Kimmel, 1990). During internalization the blastula transitions from a single blastoderm layer of cells to a gastrula consisting of epiblast and hypoblast layers. As gastrulation progresses C&E cell movements begin (Figure 2A). These movements narrow and lengthen the dorsoventral body axis of the embryo (Wallingford et al., 2002). Concluding at tailbud stage, gastrulation ultimately is responsible for the formation of three new cell layers- the ectoderm, mesoderm, and endoderm (Figure 2B).

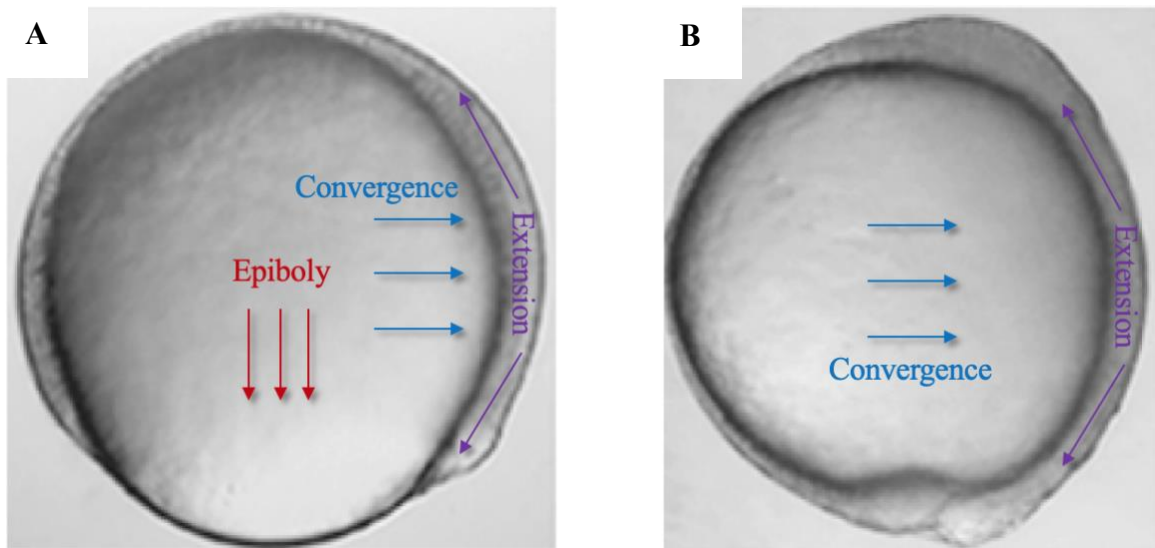


Figure 2. Cell movements during zebrafish gastrulation: (A) At mid-gastrulation (80% epiboly), epibolic movements are occurring as cells move towards the vegetal pole to cover the yolk cell. C&E movements are occurring greater now as the future dorsal axis is being built. (B) At late gastrulation (tailbud stage), the yolk cell is completely covered by cells and C&E movements continue to occur into segmentation stages.

1.1.1 Epiboly

Epiboly begins during the blastula stage when the cells (blastomeres) located on top of the yolk cell at the animal pole begin to migrate vegetally in order to close the blastopore and build an embryo with multilayers. Before the epiboly commences, the embryo consists of three cell layers: the enveloping layer, deep cells, and a yolk syncytial layer. Epiboly begins approximately 4 hours after fertilization at dome stage, when the yolk cell projects upward into the blastoderm creating a dome-like appearance (Bruce, 2016). From dome stage forward, epiboly stages are named for the percentage of the yolk cell covered by the migrating blastoderm cells. Drivers of epibolic movements have been attributed to an actomyosin and microtubule network located in the yolk cell both aiding to close the blastopore (Trinkaus, 1951; Solnica-Krezel and Driever, 1994).

During epiboly, one side of the blastoderm becomes noticeably thicker at approximately 50% epiboly or shield stage. This thickened side marks the dorsal side of the embryo (Schmitz and Campos-Ortega, 1994). At approximately 50% epiboly, a thickening also occurs at the blastoderm margin called the germ ring. This marks the beginning of internalization and also the onset of gastrulation (Figure 2A,B).

1.1.2 Internalization

Marking the official beginning of gastrulation at 55% epiboly or shield stage, cells begin to undergo internalization, whereby the future mesoderm and endoderm cells move beneath the cells of the ectoderm. This creates two layers: an outer layer of ectodermal cells (epiblast) and an inner layer of mesendodermal cells (hypoblast) which ultimately gives rise to the mesoderm and endoderm. Initially, cells of the blastoderm migrate

vegetally to internalize at the margin. After internalization, hypoblast cells begin to move anteriorly creating a multilayered embryo.

Also occurring during this time period is the formation of the germ ring and embryonic shield. The formation of the germ ring is described as a piling of internalized cells at the margin. All the while, epibolic movements are continuing until the yolk cell is entirely covered. It is not known whether internalization occurs via involution or ingression. Some studies indicate ingression movements in the dorsal region (Carmany-Rampey and Schier, 2001) and involution in the ventral. The embryonic shield is formed by intercalation of epiblast and hypoblast cells on the future dorsal side of the embryo. The zebrafish embryonic shield is the equivalent to the Spemann-Mangold organizer of amphibians which is involved in cell differentiation and patterning (Harland and Gerhart, 1997). Hypoblast cells continue to move anteriorly until approximately 76% epiboly when they take on dorsally oriented movements (Sepich et al., 2005) (Figure 2B), which is described in the next section.

1.1.3 Convergence and Extension

The last major morphogenetic cell movement pattern occurring during gastrulation is C&E. Here, cells converge towards the dorsal midline and extend anteriorly/posteriorly to form the body axis of the embryo (Figure 2B). The majority of C&E movements occur during gastrulation; however, these movements also continue into segmentation stages. Among the morphogenetic cell movements occurring during gastrulation, only C&E is reliant on PCP proteins. *vangl2* mutants show C&E defects (Jessen et al., 2002), but these embryos are able to successfully complete epiboly and internalization (Ho and Kane, 1990; Marlow et al., 1998; Solnica-Krezel et al., 1996).

C&E occurs in varying degrees across the embryo. Three domains exist along the dorsoventral axis: a dorsal domain of strong extension with little convergence, a lateral domain with increasing C&E movements, and a ventral domain which lacks C&E movements (Solnica-Krezel and Sepich, 2012). For this reason, in our studies we focus on the lateral domain which has the strongest C&E cell movements. Multiple cellular behaviors coordinate to influence C&E in the zebrafish embryo: directed migration, radial intercalation and mediolateral intercalation. In addition, extracellular matrix (ECM), cell-cell adhesion, and cytoskeletal assembly molecules have been shown to regulate C&E movements, but their interaction with PCP proteins remains a subject of interest.

1.2 Planar Cell Polarity

Key to the zebrafish PCP pathway are the proteins Glypican4 and Vangl2. Although not a core PCP protein, *glypican4/knypek* mutant embryos exhibit a severe C&E phenotype, characterized by a shortened and broadened dorsoventral body axis (Topczewski et al., 2001) (Figure 3). Glypican4 is a glycosylphosphatidylinositol (GPI) membrane-linked cell surface protein that is thought to act as a co-receptor for Wnt ligand binding to Frizzled receptors (Ohkawara et al., 2003). Downstream effectors Dishevelled and Rho family GTPases are thought to be activated by Wnt/Glypican4 signaling and ultimately influence effectors of the actin cytoskeleton. Parallel to this pathway is Vangl2, a four-pass transmembrane protein that recruits the cytoplasmic protein Prickle1 to the membrane for binding.

At the core of PCP signaling, is reorganization of the actin cytoskeleton. Members of Rho family GTPases, Rho, Rac, and Cdc42, are known to influence actin reorganization. Wnt/Glypican4/Frizzled signaling stimulates the formation of a complex between

Dishevelled, RhoA, and Daam1 resulting in RhoA activation which is shown to be required for mediolateral elongation of frog gastrula cells and lamellipodia formation (Habas et al., 2001). Wnt/Frizzled signaling also stimulates Rac, which together with Cdc42 supports actin polymerization to facilitate membrane protrusion formation and cell polarity (Schlessinger et al., 2009) (Figure 4).

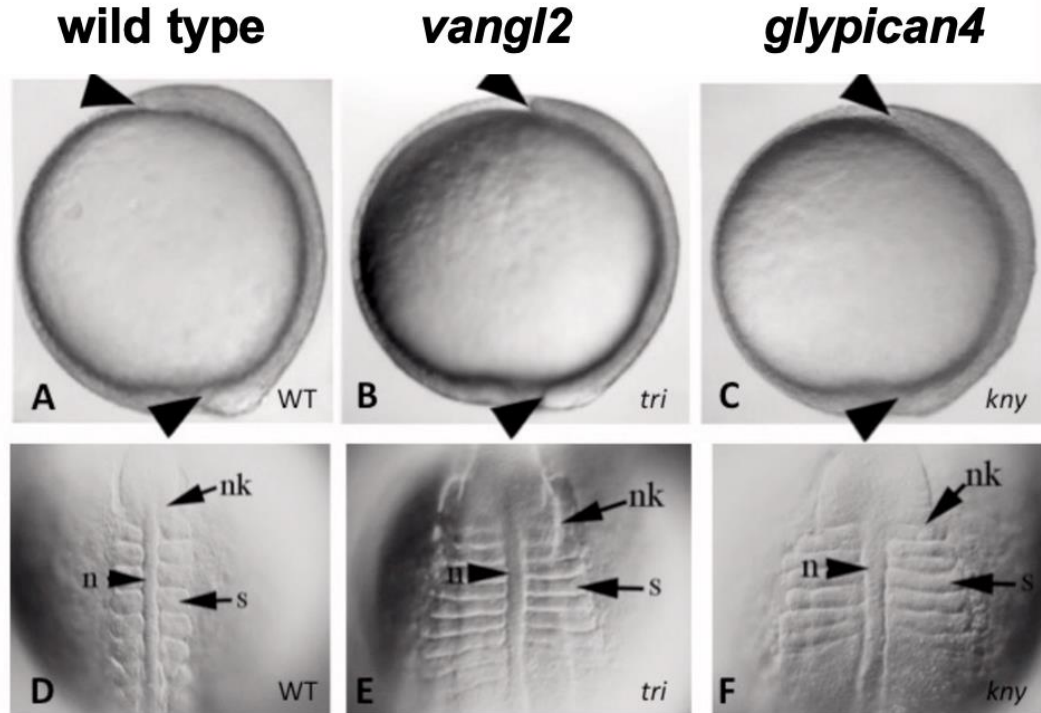


Figure 3. Zebrafish PCP mutant phenotypes: *vangl2* and *glypican4* mutant embryos exhibit a C&E phenotype compared to wild-type embryos. Lateral orientation differential interference contrast (DIC) whole mount embryo images show extension defect in PCP mutants (A-C). Dorsal DIC images show convergence defect in PCP mutants compared to wild type (D-F). *kny*, knypek. *n*, notochord. *nk*, neural keel. *s*, somite. *tri*, trilobite. *wt*, wild type.

Image credit: Marlow et al., 1998

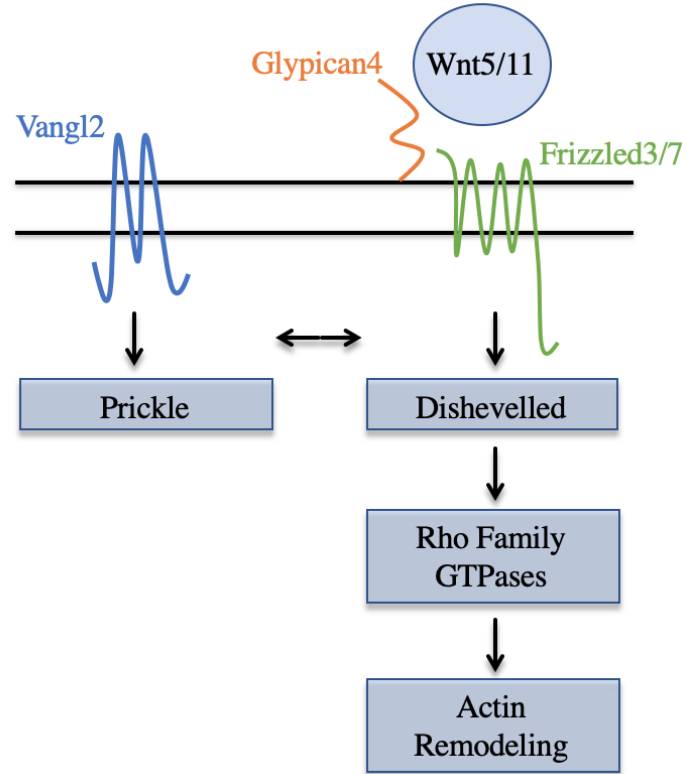


Figure 4. Vertebrate PCP signaling pathway: Wnt ligand forms a complex with transmembrane protein Frizzled and Wnt co-receptor Glypican4. The cytoplasmic protein Dishevelled signals to Rho GTPases, functioning as downstream effectors of actin remodeling. Parallel to the Wnt/Frizzled portion of the PCP pathway is four-pass transmembrane protein Vangl2 which binds Prickle. The bidirectional arrow represents crosstalk between the two sides of the pathway.

1.3 Significance of PCP Studies

Since the discovery of fly PCP protein homologs in frog, studies have continued to implicate the PCP pathway in multiple vertebrate systems. For example, mouse *vangl2* mutants exhibit forms of rachischisis meaning their neural tube remains partially or fully open to the environment (Kibar et al., 2001). Moreover, *vangl2* mutations have been linked to neural tube defects in humans (Lei et al., 2010). In addition to neural tube defects, PCP has been linked to processes such as lung branching and ciliogenesis, cilia beating in brain ventricles and trachea, and misappropriation in certain cancer cells (reviewed in Devenport, 2014).

It is hypothesized that certain cancer cells have the capacity to hijack the PCP signaling pathway in order to gain cell motility and promote cancer cell metastasis (Corda and Sala, 2017). Cell culture studies show overexpression of Wnt5a in melanoma and gastric cancer cell lines stimulates increased cell migration and metastasis (Kurayoshi et al., 2006; Weeraratna et al., 2002). Additionally, Vangl2 overexpression in breast cancer cells is linked to tumor cell proliferation (Puvirajesinghe et al., 2016). Lastly, studies by the laboratory of D. Langenau also show Vangl2 is expressed in Rhabdomyosarcoma (RMS), and when inhibited reduced cell proliferation of the RMS cancer cells was observed (Hayes et al., 2018). Therefore, a better understanding of PCP protein function could improve our understanding of human diseases such as neural tube disorders and metastatic cancers.

1.4 Membrane Protrusions Produced by Zebrafish Gastrula Cells

As cells migrate, they form a variety of plasma membrane protrusions that function as structures that can aid in sensing of the extracellular environment, gaining traction while

migrating, and communicating with neighboring cells. Filopodia, larger pseudopodia, and blebs are the most prevalent types of protrusions formed during zebrafish gastrulation (Figure 5) (Love et al., 2018).

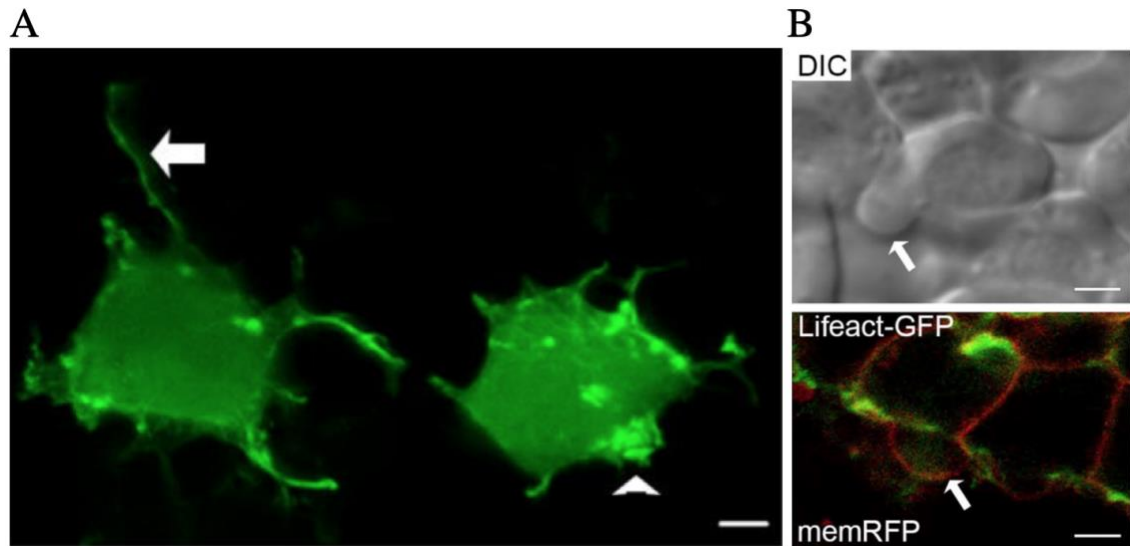


Figure 5. Protrusion types formed during zebrafish gastrulation: (A) Confocal live cell images of zebrafish mesodermal gastrula cells with arrow showing filopodia and an arrowhead showing a large protrusion labeled with Lifact-GFP. (B) DIC and confocal live cell imaging of zebrafish mesodermal cells showing bleb protrusions denoted by the arrow. Confocal fluorescent imaging is labeled with Lifact-GFP (green) and memRFP (red). Scale bars, 5 μm .

Filopodia and lamellipodia are both projections of the cell membrane that are driven by actin polymerization. Filopodia are spike-like projections of the cell membrane composed of parallel bundles of actin (Figure 5A). This type of protrusion is primarily used to sense the ECM (Abercrombie et al., 1970; Mejillano et al., 2004). In addition, filopodia have been shown to play a role in cell-cell and cell-ECM adhesion. Integrins and cadherins have been shown to be located in filopodia, presumably to promote cell adhesion and migration (Mattila and Lappalainen, 2008). Lamellipodia are sheet-like extensions of the cell formed from branched actin that are used to traction (Figure 5A).

Rho family GTPases are known to influence the organization of the actin cytoskeleton by signaling effectors to cause polymerization and branching. RhoA, Rac1, and CDC42 are the most studied of the Rho family of GTPases. Although Rho family GTPases are required for membrane protrusion formation, they do not directly modify the actin cytoskeleton. This is accomplished by signaling to actin effector proteins by specific Rho GTPases in order for actin polymerization to occur. For example, filopodia and lamellipodia formation has been shown to require the activity of actin effector protein, Arp2/3, which is activated downstream of the Rho GTPase Rac.

Blebs on the other hand, are spherical protrusions whose formation is not driven by actin polymerization. In fact, blebs are initially devoid of actin (Rottner et al., 2017) (Figure 5B). Blebs form when the plasma membrane separates from cortical actin thought to be as a result of actomyosin contractility and hydrostatic pressure (Fackler and Grosse, 2008). The bleb-cycle consists of 3 phases: initiation, expansion, and retraction. In the initiation phase, a local decrease in membrane-to-cortex attachment is observed. This detachment, thought to result from an increase in intracellular pressure, causes a bleb to form. After

bleb expansion, it continues to expand until actin filaments are rapidly assembled. Thereafter, the bleb protrusion is retracted by actomyosin contraction after the recruitment of myosin to the actin filaments (Ikenouchi and Aoki, 2016). Unlike actin-based protrusions, blebs do not appear to express integrins on the cell membrane (Diz-Muñoz et al., 2010). Data from *in vitro* studies suggested bleb protrusions typically formed in low matrix adhesion environments, whereas in high adhesion environments actin-based protrusions were the typical protrusion type formed (Tozluoğlu et al., 2013). It is also suggested membrane-cortex attachment proteins, such as members of the ERM family, could influence the formation of blebs. Interestingly, certain cell types, such as zebrafish primordial germ cells, use blebs as their primary protrusion type (Paluch and Raz, 2013), while other cell types, such as metastatic cancer cells, are able to modify their mode of migration in order to better navigate different environments and promote migration (Friedl, 2004).

1.5 Adhesive Proteins- Fibronectin and Cdh2

During the collective migration of gastrula cells, cell-cell adhesion protein, cadherins, may function to control interactions and maintain communication with neighboring cells. Cadherin1 (Cdh1) and Cadherin2 (Cdh2) are the only classical cell-cell adhesion proteins expressed during zebrafish gastrulation (Thisse et al., 2005). Both are calcium-dependent, single-pass transmembrane proteins that are characterized by five extracellular cadherin-repeat domains (Takeichi et al., 1988). Cadherin proteins undergo homophilic binding, mediated by the first extracellular domain (Nose et al., 1990) (Figure 6). Studies in zebrafish show Cdh1 is required for epiboly movements and is expressed in the ectoderm of the zebrafish gastrula. The Cdh1 mutant *half baked* exhibits arrested

epiboly movements and is embryonic lethal at 10 hours post-fertilization (Kane et al., 1996, 2005; McFarland et al., 2005). However, Cdh2 is broadly expressed in the mesoderm of the zebrafish gastrula, and loss of function Cdh2 mutants (*parachute*, *N-cadm117*) display a slight C&E defect (Harrington et al., 2007). Furthermore, a Cdh2 gain of function mutant (*biber*, *bib^{ts8}*) exhibits a modest C&E phenotype, suggestive of a possible molecular interaction with PCP proteins during C&E cell movements (Warga and Kane, 2007). Previous studies demonstrate during mouse synapse formation that Vangl2 directly binds Cdh2 and influences Cdh2 internalization (Nagaoka et al., 2014). Additionally, it is known the PCP signaling pathway influences actin cytoskeleton dynamics, and classical cadherins are structurally linked to the actin cytoskeleton by alpha- and beta-catenin. Signaling to the actin cytoskeleton is in part mediated by recruitment of p120-catenin upon cadherin-cadherin binding. In cell culture studies, it is shown at the area of cell-cell contact p120 activates Rac thereby inhibiting RhoA. Alpha-catenin has effects on Arp2/3 which can interfere with actin polymerization (Maître and Heisenberg, 2013).

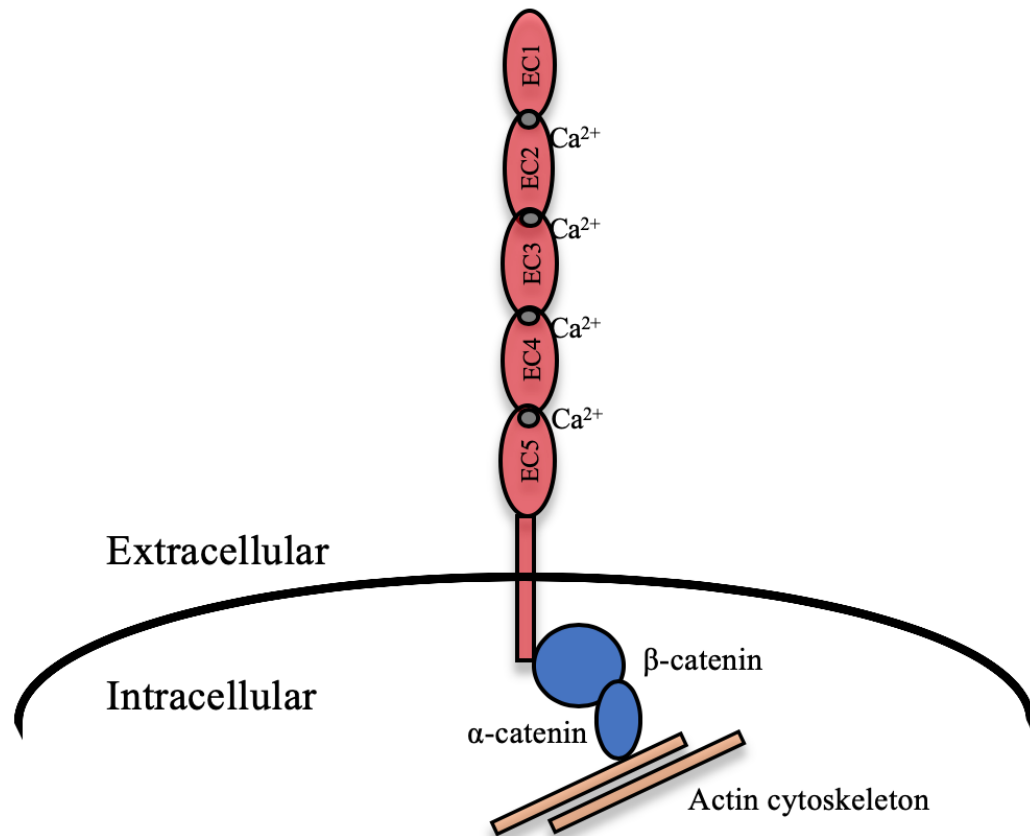


Figure 6. Structure of classical cadherins: Classical cadherins are single-pass transmembrane proteins that function as cell-cell adhesion molecules. Classical cadherins contain five extracellular (EC) domains (red) on the extracellular side. Calcium ions (Ca²⁺) bind between each EC domain during activation (grey). On the intracellular side, α - and β -catenin (blue) mediate the interaction with the actin cytoskeleton (yellow).

During zebrafish gastrulation, cells interact with and migrate upon a cell-secreted ECM. Commonly found ECM proteins include collagen, laminin, elastin, and fibronectin. These macromolecules are secreted by the cells and organized into a meshwork mediated by specific ECM receptors on the cell surface (reviewed in Jessen, 2015). Fibronectin, laminin, and collagen transcripts are all detected in zebrafish gastrulae. However, laminin knockdown in zebrafish does not produce a C&E defect, and collagen is restricted to the axial tissues during zebrafish gastrulation (Thisse et al., 2004). Thus, for the purposes of my dissertation I focused on fibronectin.

Fibronectin is the major ECM protein present during zebrafish gastrulation (Latimer and Jessen, 2010). It is established in other vertebrate model organisms that fibronectin is crucial for gastrulation cell movements. For instance, proper polarity of membrane protrusions requires a fibronectin ECM in the frog and loss of function of fibronectin produced misshapen frog gastrula embryos (Skoglund and Keller, 2010). In the mouse embryo, loss of function of fibronectin is embryonic lethal due to mesoderm defects (George et al., 1993). Unlike the frog and mouse, the requirements of a fibronectin ECM in zebrafish embryos are not well understood.

In zebrafish, there are two fibronectin isoforms: Fibronectin1a and Fibronectin1b (Sun et al., 2005; Zhao et al., 2001). Fibronectin expression first becomes apparent at approximately 65% epiboly and is restricted to the epiblast-hypoblast boundary (Latimer and Jessen, 2010). Expression and fibrillogenesis, crosslinking of fibronectin fibrils, increases as gastrulation proceeds with a new layer of fibronectin occurring beneath the mesendodermal cells. Ultimately by the end of gastrulation, two distinct layers of

fibronectin ECM are present, at the ectoderm-mesoderm boundary and beneath the cells of the deep mesoderm.

Loss of fibronectin function results in zebrafish embryos with a slight C&E defect (Love et al., 2018). Until recently, the role of fibronectin in establishing PCP was unclear. However, our previously published data (Love et al., 2018) details the contribution of fibronectin to proper membrane protrusive activity. Fibronectin is secreted by the cell as a dimer joined by a disulfide bond. It is comprised of type I, II, and III repeating units, and sets of these units represents binding domains for either cells or specific ECM proteins (Wierzbicka-Patynowski and Schwarzbauer, 2003). In solution fibronectin is a compact, folded structure that will not undergo fibril assembly. Cell surface receptors called integrins are responsible for binding cells to the ECM and required for activating fibronectin in order to assemble fibrils. Structurally, an Arginine-Glycine-Asparagine (RGD) sequence is required for integrin binding (Sechler et al., 1996), and there are at least four known subunits that exist for fibronectin-fibronectin binding (Wierzbicka-Patynowski and Schwarzbauer, 2003) (Figure 7).

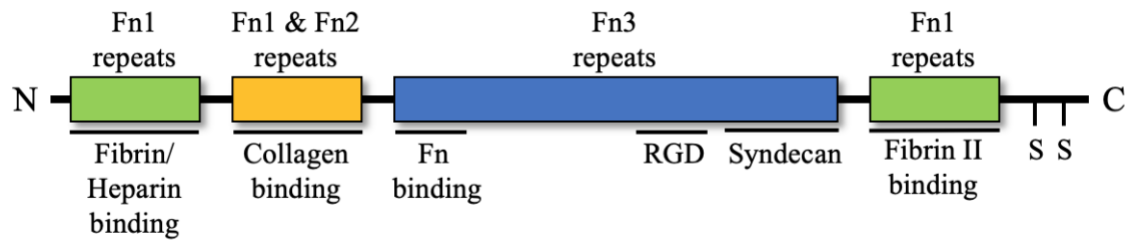


Figure 7. Structure of fibronectin: Fibronectin consists of type I (green), type II (yellow), and type III (blue) repeats. Black lines denote regions of binding for Fibrin, Heparin, Collagen, Fibronectin (Fn), and Syndecan, as labeled. RGD represents amino acid sequence where integrins bind. S-S represents sulfide bonds that facilitate dimer formation.

Interestingly, zebrafish *vangl2/trilobite* and *glypican4/knypek* mutants have differential cadherin and fibronectin phenotypes. *vangl2/trilobite* mutant embryos have decreased cadherin expression on the cell surface and a decrease in fibronectin fibrillogenesis (Dohn et al., 2013; Williams et al., 2012). Here, fibronectin protein levels are decreased as indicated by western blot. This is likely due to a decrease in actomyosin contractility and increased matrix metalloproteinase (MMP) activity (Dohn et al., 2013; Williams et al., 2012).

By contrast, *glypican4* mutants have increased cell surface expression of cadherin proteins thought to be due to disrupted vesicular trafficking correlating with an increase in fibronectin fibrillogenesis. By western blot, this is shown not to be due to an increase in total protein levels of Cdh1 and Cdh2 (Dohn et al., 2013). Supported by data from frog, this phenotype is likely due to *glypican4* mutants having an increase in fibronectin assembly as a result of integrin-fibronectin binding. This model proposes that cadherin-generated mechanotension transfers force through the actin cytoskeleton to integrins, which is necessary to expose cryptic sites on fibronectin that promote homophilic interactions (Dzamba et al., 2009).

1.6 Dissertation Goal

The goal of my dissertation is to characterize the transition from PCP-independent to PCP-dependent cell behaviors that occurs from mid- to late gastrulation during zebrafish development. At mid-gastrulation, ectodermal and mesodermal cells are rounder and lack mediolateral alignment and cohesion. By late gastrulation, these properties have changed. Cells are now elongated and have increased mediolateral alignment and cohesion, suggesting a role for PCP proteins. Influences underlying this transition are not known. We

hypothesize changes in membrane-protrusive activity influence this transition. In addition, we hypothesize changes in the expression of the cell-ECM protein, fibronectin, and cell-cell adhesion protein, *Cdh2*, influence this transition also. The work described here examines the change in protrusive activity from mid- to late gastrulation and the requirement of adhesion proteins for PCP-dependent cell behaviors.

To do this, membrane protrusions will be quantified by fluorescent confocal and DIC microscopy at mid- and late gastrulation, and *vangl2* mutant embryos will be used to determine the requirement of *Vangl2*, similarly. Next, DIC time-lapse imaging will be used to determine if adhesion proteins, fibronectin and *Cdh2*, are required for PCP and the directed migration of mesodermal gastrula cells. Lastly, a series of transplantation experiments will be performed to determine if *vangl2* regulates protrusion formation cell autonomously or non-autonomously.

CHAPTER TWO. Vangl2 is Required for Polarization of Filopodia at Late Gastrulation

2.1 Introduction

Mesendodermal cells adopt dorsally-biased migration trajectories at approximately 75% epiboly (Sepich et al., 2005). Mesendodermal cells are located in the hypoblast and give rise to the mesoderm and endoderm, which becomes two distinct cell layers by late gastrulation. At mid-gastrulation, mesendodermal cells do not exhibit PCP hallmarks and migrate toward the dorsal axis with meandering trajectories (Jessen et al., 2002). These cells also have reduced cohesion (meaning there are increased gaps between cells and less cell-cell contacts) compared to later gastrulation stages, and Vangl2 function is not required for these early gastrulation cell movements (Jessen et al., 2002; Sepich et al., 2005). By late gastrulation the now termed deep mesodermal cells exhibit PCP-dependent polarized behaviors shown by increased cellular length-width ratios (LWR) and mediolateral alignment (MLA) (Jessen et al., 2002; Topczewski et al., 2001). This change is accompanied by an increase in cohesion and a straightening of migration trajectories. Our previous data shows that zebrafish ectodermal cells at late gastrulation stage typically only generate filopodia-like and large protrusions and form very few bleb-like protrusions (Love et al., 2018). Additionally, it was shown Vangl2 is required for proper regulation of membrane protrusions of zebrafish ectodermal cells (Love et al., 2018).

Although we now know Vangl2 is needed for proper membrane-protrusive activity of ectodermal gastrula cells at late gastrulation, it is not known if Vangl2 is required for mesodermal cell protrusive activity. Additionally, protrusive details underlying the transitional period from PCP-independent to PCP-dependent movements in mesodermal

gastrula cells from mid- to late gastrulation is not understood. We aimed to characterize membrane-protrusive activity at 80% epiboly (mid-gastrulation) and tailbud (late gastrulation) developmental stages. We hypothesized a shift in membrane protrusive activity contributes to the transition to polarized cell behaviors occurring from mid- to late gastrulation stages.

2.2 Results

Mesodermal cells have increased filopodia at late gastrulation

First, we aimed to quantify membrane protrusion types to characterize membrane protrusive activity of mesodermal cells. The stages of 80% epiboly (mid-gastrulation) and tailbud (late gastrulation) in wild-type embryos were used. Actin-based protrusions (non-blebs) were analyzed by mosaic expression of Lifeact-GFP to label actin without interference of labelling from neighboring cells and confocal microscopy. Mosaic expression of mesodermal cells was obtained by injecting a single blastomere at 8-cell stage. Imaging of lateral mesoderm was performed 90 degrees from the notochord for tailbud stage embryos and 40-60 degrees for 80% epiboly stage embryos. This is due to paraxial/pre-somitic mesoderm exhibiting different cell behaviors compared to lateral mesoderm cells engaged in directed migration (Williams et al., 2012). Protrusions were broadly classified as filopodia (white arrow) or large protrusions (white arrowhead) (Figure 8A). We found there was a significant increase in the number of filopodia per cell from 80% epiboly to tailbud stages (Figure 8B). By contrast, there was not a significant difference in large protrusion formation between mid-gastrulation to late gastrulation in wild-type embryos (Figure 8C). *vangl2* mutant embryos were also analyzed at tailbud stage for comparison to wild-type embryos. *vangl2* mutant embryos were only analyzed at

tailbud stage because the requirement for Vangl2 is not evident until late gastrulation when a phenotype is present. We found *vangl2* mutant mesodermal cells had similar levels of filopodia per cell compared to wild-type tailbud stages indicating Vangl2 is not required for filopodia production in mesodermal cells (Figure 8B). When analyzing large protrusions, we also did not find a difference in *vangl2* mutant mesoderm compared to wild-type control cells (Figure 8C).

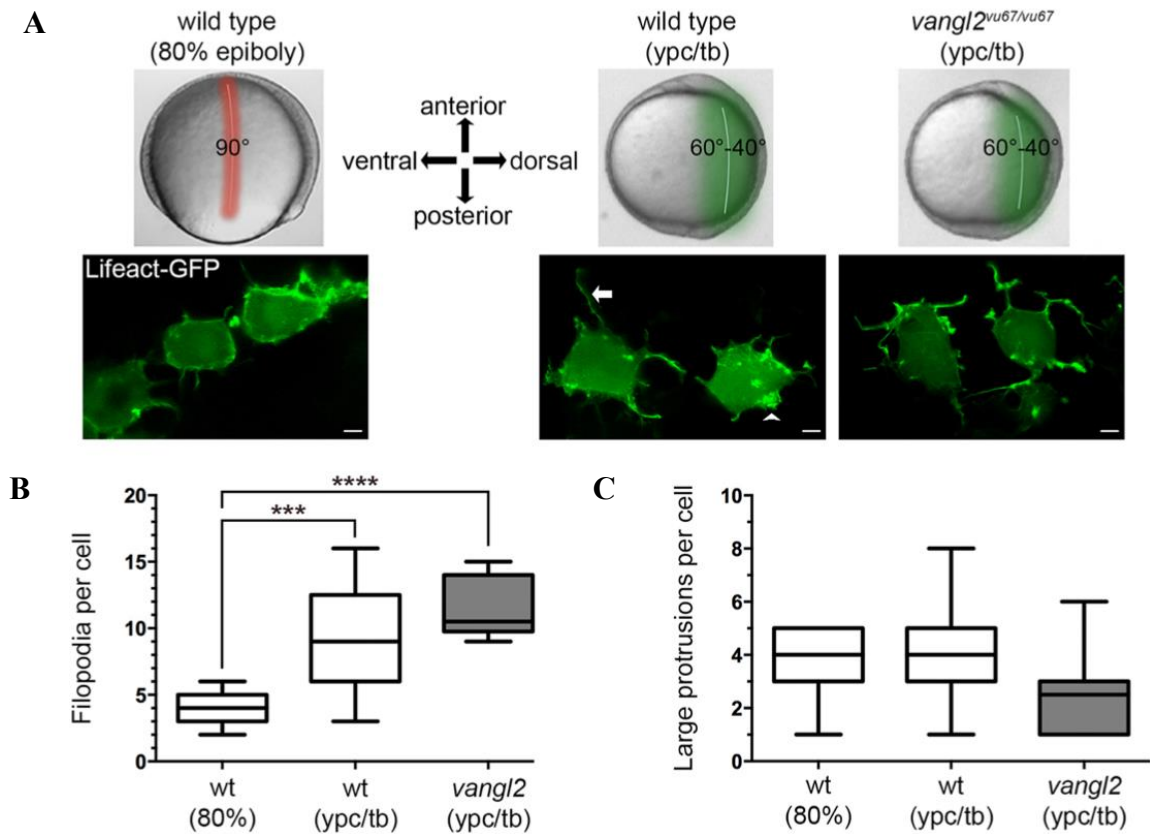


Figure 8. Greater filopodia production at late gastrulation: (A) Whole mount images of wild-type embryos at 80% epiboly and tailbud stage and *vangl2^{vu67/vu67}* mutant tailbud stage embryos. Shading represents approximate areas of imaging. Also shown are fluorescent confocal time-lapse images from each represented stage showing mosaic expression of Lifeact-GFP. White arrow labels filopodia and white arrowhead labels a large protrusion. Scale bars, 5 μ m. **(B)** Filopodia production of mesendodermal cells (80% epiboly) from wild-type embryos and mesodermal cells (tailbud) from wild-type and *vangl2^{vu67/vu67}* mutant embryos (wt 80% epiboly, n=7, 6 embryos; wt tb, n=13, 10 embryos; *vangl2* mutant, n=10, 6 embryos). **(C)** Large protrusion production of mesendodermal cells (80% epiboly) from wild-type embryos and mesodermal cells (tailbud) from wild-type and *vangl2^{vu67/vu67}* mutant embryos. Box plots display data as the interquartile dataset, the median, and the data range. * $P < 0.05$, *** $P < 0.001$, **** $P < 0.0001$; unpaired Student's t-test with Welch's correction. Ypc/tb, yolk-plug closure/tailbud stage.

Vangl2 is required for polarized filopodia in mesodermal cells

To determine if there was a difference in the polarity of the protrusions formed, we next quantified polarity of membrane protrusions in relation to the path of dorsal migration. Polarity was defined as being ± 45 degrees from a line drawn through the cell and perpendicular to the notochord. Polarity was displayed as dorsal only or ventral+dorsal referring to whether the protrusion was formed from the ventral/trailing edge or dorsal/leading edge. We found no difference in the polarity of leading edge/dorsal protrusions between 80% and tailbud stage embryos (Figure 9A). Polarity of large protrusions was highly variable between cells between mid- to late gastrulation and showed no difference (Figure 9B). Interestingly, we did find that mediolaterally-biased (ventral+dorsal) filopodia was significantly increased at late gastrulation of wild-type cells indicating a majority of filopodia were oriented at the trailing edge (Figure 9A). Next, analysis of *vangl2* mutant mesodermal cells revealed the polarity of filopodia (ventral+dorsal) was significantly decreased in *vangl2* mutant embryos compared to wild-type suggesting Vangl2 is required for proper polarity of filopodia at late gastrulation (Figure 9A).

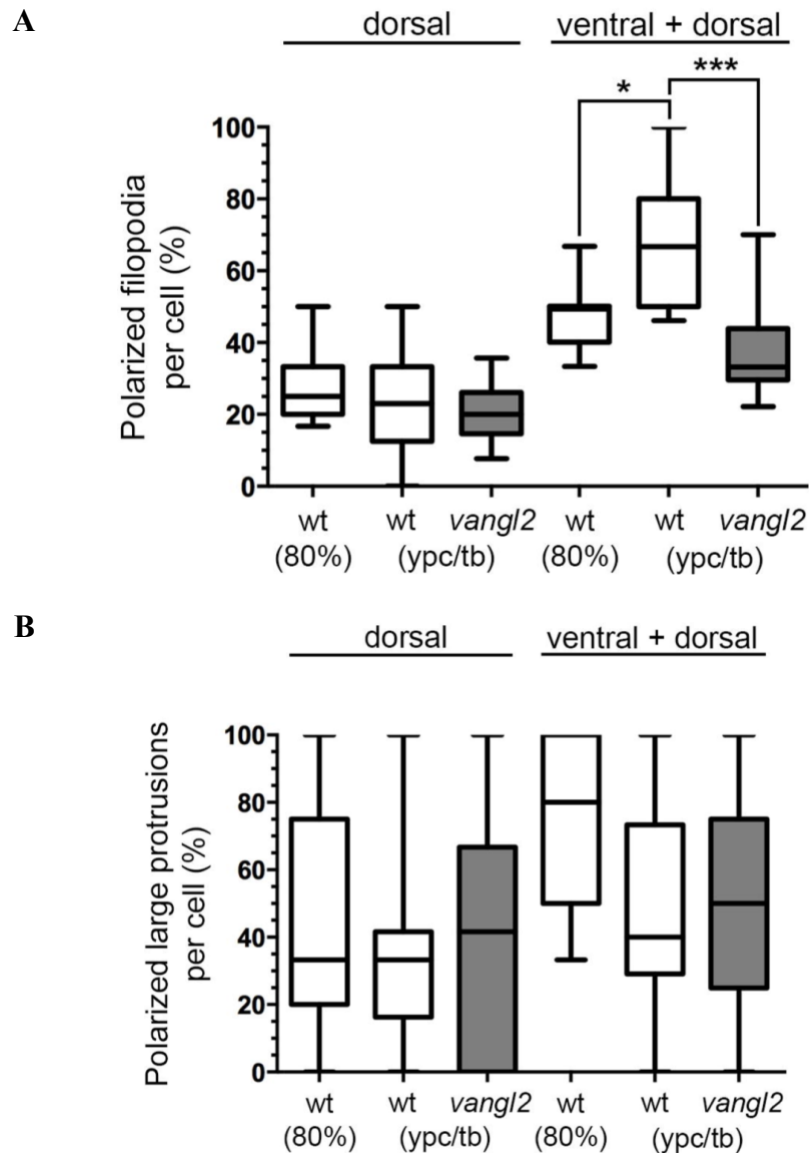


Figure 9. Vangl2 is needed for polarization of filopodia at late gastrulation: (A) Percentage of polarized filopodia per cell from wild-type 80% epiboly and tailbud stage and *vangl2*^{vu67/vu67} mutant tailbud stage embryos. Polarization is shown as dorsal edge only and ventral + dorsal edge (wt 80% epiboly, n=7, 6 embryos; wt tb, n=13, 10 embryos; *vangl2* mutant, n=10, 6 embryos). **(B)** Percentage of polarized large protrusions per cell of wild-type mesendodermal cells and mesodermal cells from wild-type and *vangl2*^{vu67/vu67} mutant embryos. Polarization is shown as dorsal edge only and ventral + dorsal edge. Box plots display data as the interquartile dataset, the median, and the data range. *P<0.05, ***P<0.001, ****P<0.0001; unpaired Student's t-test with Welch's correction. Ypc/tb, yolk-plug closure/tailbud stage.

2.3 Conclusion

In this section, we aimed to characterize membrane-protrusive activity of wild-type mesendodermal and mesodermal cells undergoing the transition from PCP-independent to PCP-dependent cell behaviors. We also aimed to analyze *vangl2* mutant mesodermal cells to determine the requirement of Vangl2 for actin-based protrusion formation. First, we found mesodermal cells at late gastrulation have greater filopodia production compared to mesendodermal cells at mid-gastrulation. We hypothesize this could be due to a normally occurring increase in the fibronectin ECM from mid- to late gastrulation (Latimer and Jessen, 2010) and these protrusions are more productive in higher ECM environments.

Next, when analyzing *vangl2* mutant mesodermal cells, we found they exhibited levels not significantly different from that of wild-type mesodermal cells at late gastrulation. This suggests the increase in filopodia occurring from mid- to late-gastrulation does not require Vangl2 protein. However, differences in protrusion formation were observed when analyzing the polarity of the protrusions. It is suggested cells migrate by extending protrusions at the leading edge while simultaneously retracting the trailing edge, and typically most membrane protrusions are formed at the leading edge. We quantified polarized protrusions produced from the dorsal edge of the cell and found no significant difference between wild-type cells at 80% epiboly and tailbud stages or *vangl2* mutant cells. However, when ventral produced protrusions were combined with dorsal produced, we saw a significant increase in polarized filopodia at late gastrulation compared to mid-gastrulation suggesting more protrusions are forming at the ventral side of the cell compared to dorsal. The percentage of polarized (dorsal + ventral) in *vangl2* mutant

mesodermal cells was similar to levels seen in mesendodermal cells at 80% epiboly suggesting Vangl2 is required for proper filopodia polarity.

To summarize, we show filopodia production in mesodermal cells at late gastrulation is greater than at mid-gastrulation. Furthermore, the amount of mediolateral polarized filopodia increases from mid- to late gastrulation, and Vangl2 is required for increase in polarized filopodia at late gastrulation.

CHAPTER THREE: Mesodermal Cells Exhibit Increased Bleb Protrusions at Mid-Gastrulation

3.1 Introduction

Bleb protrusions were first identified as early as 1919 and were described as blisters or bubbles of the cell membrane (Holtfreter, 1943). Later, Trinkhaus more thoroughly analyzed blebs during early *Fundulus heteroclitus* gastrulation gaining insight on physicochemical properties in migrating deep cells of the gastrula. Initially, blebs were viewed as a byproduct of apoptotic and necrotic processes until later studies revealed blebs can be used for locomotion of certain cell types (Coleman et al., 2001).

In contrast to actin-based protrusions, bleb protrusions are initially devoid of actin filaments until shortly after formation when actin is needed for bleb retraction. Blebs have a short life span and take approximately 30 seconds to progress through the three phases of the bleb life cycle: initiation, growth, and retraction (Paluch and Raz, 2013). In our previous studies, it was discovered that zebrafish ectodermal gastrula cells form very few bleb protrusions as they migrate towards the dorsal axis (Love et al., 2018). Unlike the ectoderm, mesendodermal cells at mid-gastrulation have decreased cohesion and do not align and pack together until later stages of gastrulation. Some cells use blebs as their primary type of protrusion for migration such as zebrafish primordial germ cells as they undergo amoeboid-like cell migration during very early gastrulation stages (Paluch and Raz, 2013).

It has also been shown that mesendoderm progenitor cells that use bleb protrusions alternate between stages of runs and tumbles. Runs are characterized by increased actin-based protrusion formation and tumbles by increased bleb protrusions and decreased actin-

based protrusions (Diz-Muñoz et al., 2016). Furthermore, previous studies have shown that cancer cells adopt an amoeboid mode of migration (i.e. form blebs) when put into a 3D matrix (Sahai, 2005). Furthermore, when noninvasive cells were put into a 3D matrix, cells adopted bleb-based migration (Gadea et al., 2007). Taken together this suggests blebbing can enable cells to gain directed motility in 3D environments. In this section, we aim to characterize bleb membrane-protrusions as mesodermal gastrula cells transition from PCP-independent to PCP-dependent cell behaviors.

3.2 Results

Mesendodermal cells display greater blebbing compared to mesodermal cells

First, to determine the quantity of bleb protrusions in lateral mesodermal cells, a combination of DIC microscopy and time-lapse imaging were used to analyze mesendodermal and mesodermal cells at mid- and late gastrulation. To verify that blebs could be accurately quantified by DIC time-lapse microscopy, Lifeact-GFP and membrane-targeted RFP (memRFP) were used to label bleb protrusions using confocal time-lapse microscopy. Mosaic expression of Lifeact-GFP and mem-RFP allowed imaging of cells without interference of neighboring cells (Figure 10A). To achieve mosaic expression, a single blastomere was injected at 8-cell stage. Once we were confident we could identify blebs using DIC microscopy, time-lapse images (15 minute duration, 30 second interval) were collected (Figure 10B). We found greater bleb protrusion formation at mid-gastrulation compared to late gastrulation. This was quantified as the percentage of cells forming blebs and as blebs per cell. The percentage of cells forming bleb protrusions at 80% epiboly (17.037%) was significantly higher compared to tailbud stage (1.43%)

(Figure 11A). When quantified as the number of blebs per cell, a significant difference in blebs per cell was seen but it was not as great as the percentage of cells forming blebs (Figure 11B). An average of 1.55 blebs were formed per cell at mid-gastrulation and an average of 0.7 blebs per cell were formed at tailbud stage.

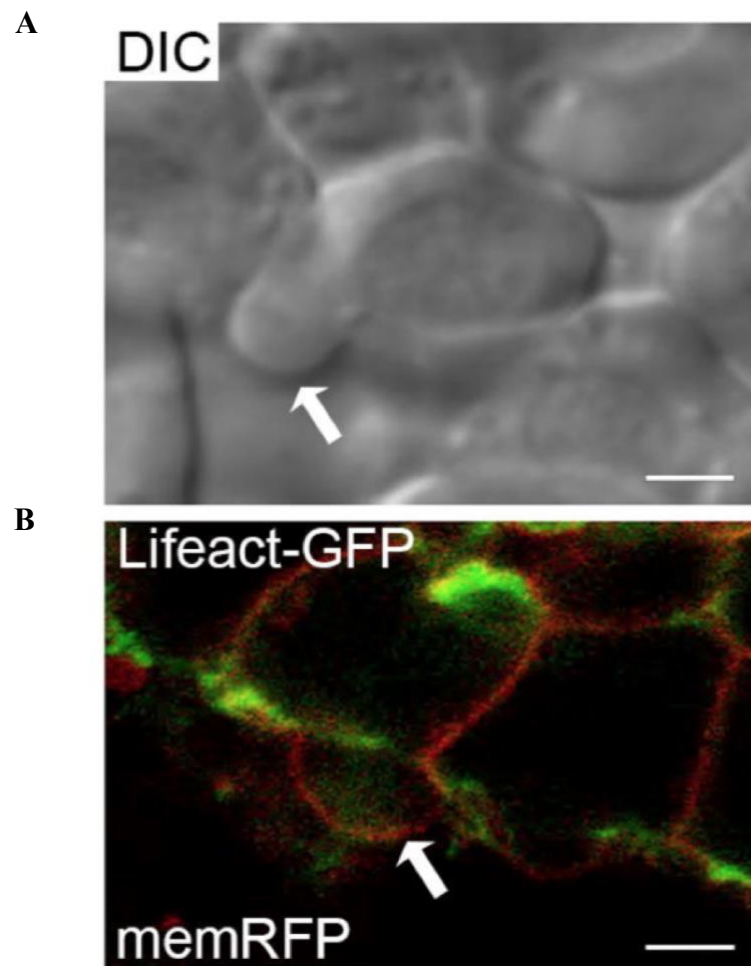


Figure 10. Bleb protrusion imaging by DIC and confocal microscopy: (A) DIC time-lapse image of mesendodermal cells at 80% epiboly. White arrow labels a bleb protrusion. (B) Confocal time-lapse image of mesendodermal cells at 80% epiboly. Cells have mosaic expression Lifeact-GFP (green) and memRFP (red). White arrow denotes a bleb protrusion. Scale bars, 5 μm .

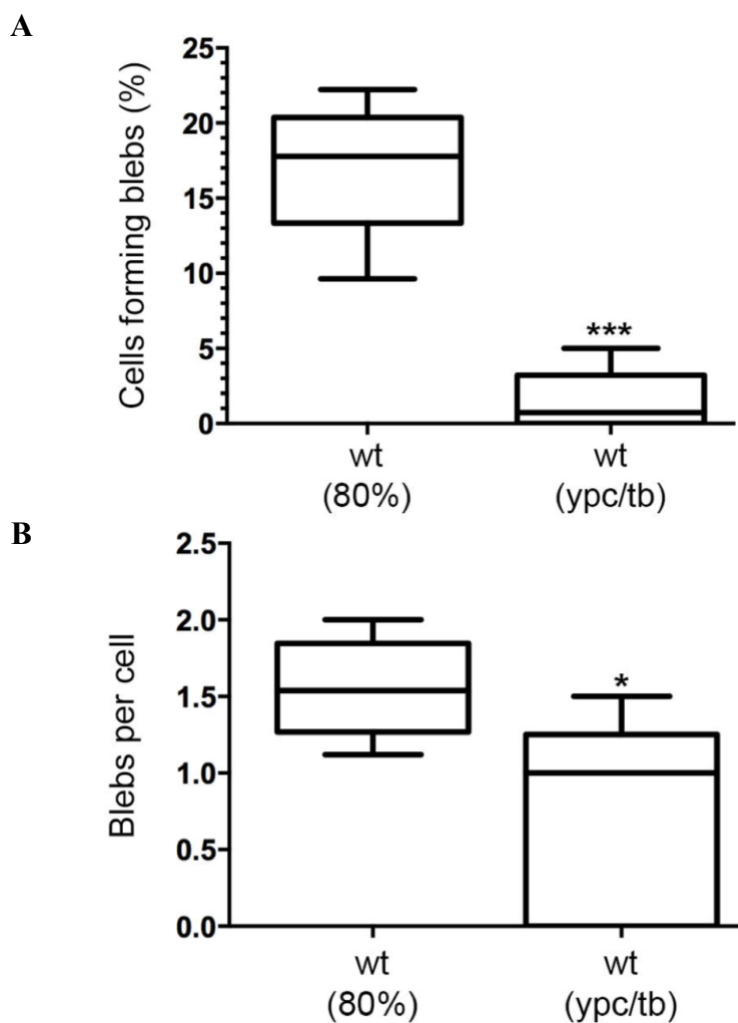


Figure 11. Increased bleb protrusions at mid-gastrulation: Bleb protrusion quantification of mesendodermal and mesodermal cells from wild-type embryos. Analysis is from 15-minute DIC time-lapse videos. Blebs are quantified as the percentage of cells **(A)** forming blebs and blebs per cell **(B)**. Box plots display data as the interquartile dataset, the median, and the data range (wt 80% epiboly, n=675 cells, 5 embryos; wt tailbud, n=700 cells, 5 embryos). *P<0.05, ***P<0.001, unpaired Student's t-test with Welch's correction. Ypc/tb, yolk-plug closure/tailbud stage.

Blebs produced by mesendodermal cells were highly polarized in run phases

Next, we analyzed the polarity of bleb protrusions from mid- to late gastrulation. To do this, a line was drawn through the cell and parallel to the path of migration. Blebs were considered polarized if they were oriented ± 45 degrees in relation to the path of migration. Path of migration was used for measuring polarity due to mesendodermal cells at mid-gastrulation having indirect cell migration trajectories. This is opposed to late gastrulation when cells exhibit more cell-cell contacts and migrate in a direct dorsal direction. The results showed the number of polarized leading edge blebs was 26.8%. This percentage indicates a lack of polarity. Dissecting this data further, cells were categorized into phases of tumbles and runs, and the polarity of blebs formed in both phases was analyzed. It is noted that blebs formed during both of these phases of mesendodermal cell migration. We found that only 24% of the blebs were polarized during the tumbling phase. However, 100% of the blebs formed during run phases were polarized (Figure 12).

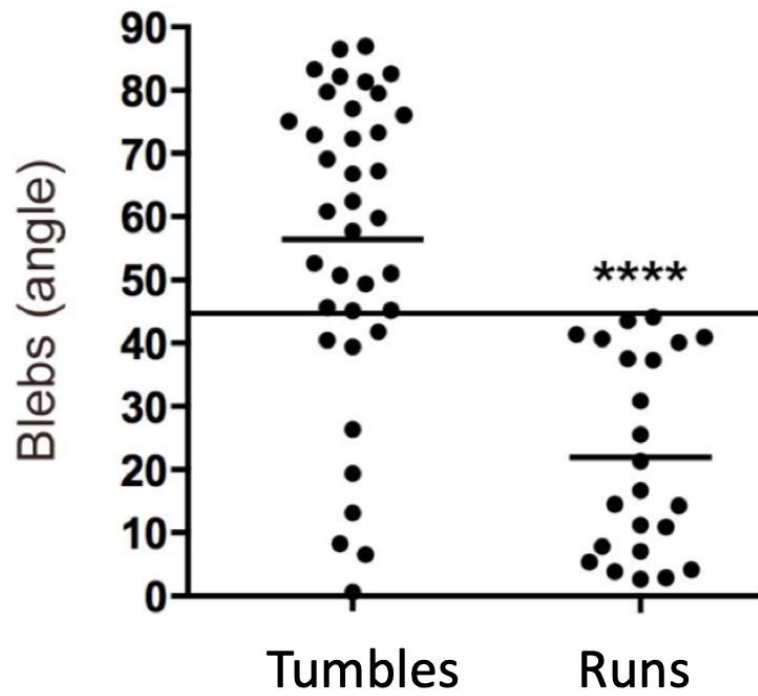


Figure 12. Mesendodermal cells produce highly polarized blebs in run phases: Bleb protrusion angles from wild-type mesendodermal cells quantified in relation to path of migration. Horizontal black line denotes 45 degrees. Scatter plot shows individual data points and average values (wt, n=25 cells, 2 embryos). ****P<0.0001, unpaired Student's t-test with Welch's correction.

Reduction in bleb protrusions from mid- to late gastrulation may be due to Ezrinb expression

Due to the differences in bleb protrusions from mid- to late-gastrulation, we proposed the established membrane-to-cortex attachment protein, Ezrinb (Ezrb), may differentially activated during gastrulation. To test this, total protein extracts from wild-type 80% epiboly and tailbud stage embryos were generated. Anti-Ezrb and anti-phosphorylated-Ezrb antibodies were used to detect total protein and activated levels of Ezrb, respectively. This revealed levels of phosphorylated-Ezrb were significantly increased in tailbud stage embryos compared to 80% epiboly stage wild-type embryos, while total protein levels of Ezrb stayed the same between stages (Figure 13A). Average band density was quantified from three experimental replicates confirming a significant increase in phospho-Ezrb from 80% epiboly to tailbud stage (Figure 13B).

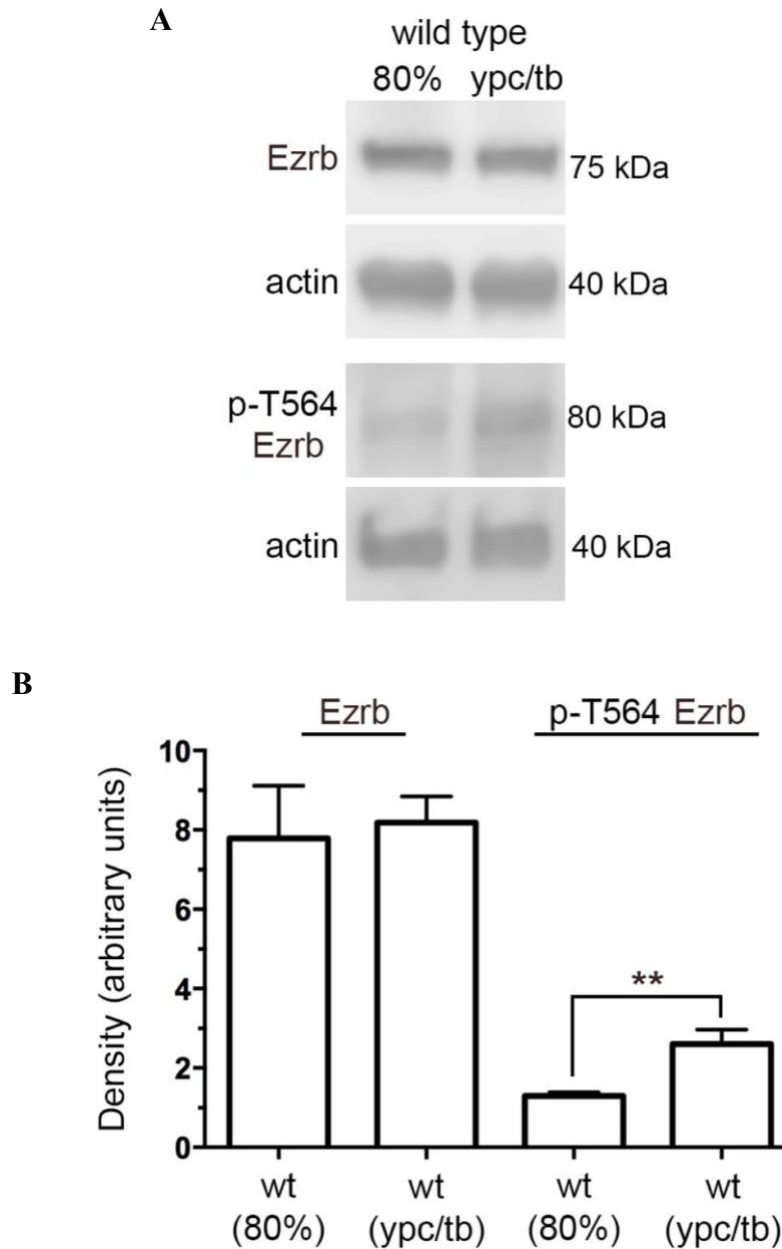


Figure 13. Increased activated Ezrinb at late gastrulation: (A) Western blot showing total protein levels (Ezrb) and phosphorylated levels of Ezrinb (p-T564 Ezrb) from 80% epiboly and tailbud stage wild-type embryos. (B) Average western blot band density quantification normalized to actin controls. Western blots were performed in triplicate as independent biological repeats. Bar graph (B) shows average values \pm the standard deviation. ** $P < 0.001$, unpaired Student's t-test with Welch's correction. Ypc/tb, yolk-plug closure/tailbud.

3.3 Conclusion

In this section, we aimed to characterize the bleb protrusive activity of mesendodermal and mesodermal cells from mid- to late gastrulation, respectively. We previously showed an increase in filopodia occurring between these stages. In contrast to our previous results, we found a decrease in the percentage of cells forming blebs from mid- to late gastrulation. Therefore, our data shows bleb protrusions are preferred at mid-gastrulation, and filopodia are preferred at late gastrulation.

Next, polarity of blebs was quantified in relation to the direction of movement. Direction of movement was considered the most accurate way to measure polarity due to mesendodermal cells exhibiting meandering trajectories to the dorsal body axis. We found that blebs were not considered polarized based on this observation. Data from early zebrafish gastrula cells undergoing anterior migration (prior to 80% epiboly) suggested actin-based protrusions (filopodia and lamellipodia) and blebs are needed for runs and tumbling phases of cell movement, respectively (Diz-Muñoz et al., 2016). Thus, we dissected bleb polarity further by classifying blebs into phases of tumbles and runs. Blebs were classified in a tumbling phase if they were stationary and as runs if they were actively migrating. We found 100% of blebs were polarized in phases of runs, and no blebs were polarized in phases of tumbles. This indicates that a combination of actin-based and bleb protrusions are necessary for dorsal convergence of lateral mesendodermal cells. Additionally, this indicates bleb protrusions are the primary protrusion when cells are reorienting themselves during migration.

We hypothesized that loss of bleb protrusions at late gastrulation could be due to decreased ezrin protein activation due to its role as a major membrane-to-cortex attachment

protein (Bretscher et al., 1997). We found by western blot that total Ezrin protein levels remained the same in 80% epiboly and tailbud staged embryos, but phosphorylated-Ezrin levels were increased in tailbud stage compared to 80% epiboly embryos.

In summary, we found mesendodermal cells produce a greater number of blebs as they undergo dorsal convergence compared to mesodermal cells. We also found bleb protrusions formed at 80% epiboly were highly polarized relative to path of migration in run phases of migration compared to tumble phases. Lastly, we found protein levels of p-Ezrin are increased in wild-type embryos at late gastrulation compared to mid-gastrulation. We propose these increased levels of p-Ezrin could explain the differences in bleb protrusions between these stages.

CHAPTER FOUR. Bleb Protrusions Inhibit PCP and Directed Migration

4.1 Introduction

Although some cells exclusively form either actin-based protrusions or blebs, other cells are able to switch protrusion types based on cellular environment and intracellular signaling. Membrane-to-cortex attachment is known to play a role in the ability of cells to form blebs (Paluch and Raz, 2013). Ezrin, the most studied of the ERM family, associates with the membrane through its N-terminal domain and cortical actin with its C-terminal (Bretscher et al., 1997). Ezrb is activated/phosphorylated at T564 (Jayasundar et al., 2012). In zebrafish, Ezrb expression is localized to the ectoderm and mesoderm of embryos during gastrulation (Link et al., 2006). Also, knockdown of Ezrb has been shown to increase bleb protrusion formation and simultaneously decrease actin-based protrusions (Diz-Muñoz et al., 2010). Furthermore, it has been shown activated *ezrin* is required for ingression and subsequent migration of early mesendodermal cells, and *ezrb* morphants displayed a slight C&E defect (Link et al., 2006) indicated a possible PCP defect.

Thus far, our data has shown bleb protrusive activity decreases from mid- to late gastrulation, and this reduction in blebbing by late gastrulation suggests this type of protrusive activity is not required or may be inhibitory for PCP-dependent mesodermal cell migration. Additionally, we have shown levels of activated Ezrb protein increases from mid- to late gastrulation. We suggest this increase in active Ezrb is responsible for the decrease of bleb protrusion formation seen from 80% epiboly to tailbud stage. Therefore, we aim to manipulate Ezrb function to determine if blebbing at late gastrulation negatively influences directed migration or PCP. Manipulation of bleb protrusions using a constitutively active form of Ezrb and knockdown by morpholino (MO) has been

previously verified in other studies to decrease and increase blebbing, respectively (Diz-Muñoz et al., 2016). We hypothesize stimulation of bleb protrusion formation at late gastrulation will be inhibitory for PCP and directed migration. By contrast, we hypothesize activation of *Ezrb* at mid-gastrulation will inhibit blebbing, thereby influencing directed migration.

4.2 Results

***Ezrinb* morphants display a C&E phenotype**

DIC time-lapse microscopy along with genetic tools to alter *Ezrb* protein function were used to analyze the effects of blebbing at late gastrulation. To determine if blebbing is inhibitory for PCP, we injected wild-type embryos with an *ezrb* MO at one-cell stage. We then performed 15-minute DIC time-lapse imaging with 30 second intervals for bleb analysis. We discovered *ezrb* morphants display a slight C&E phenotype characteristic of defective PCP indicating *Ezrb* could be required for proper PCP and directed migration of zebrafish mesodermal cells (Figure 14).

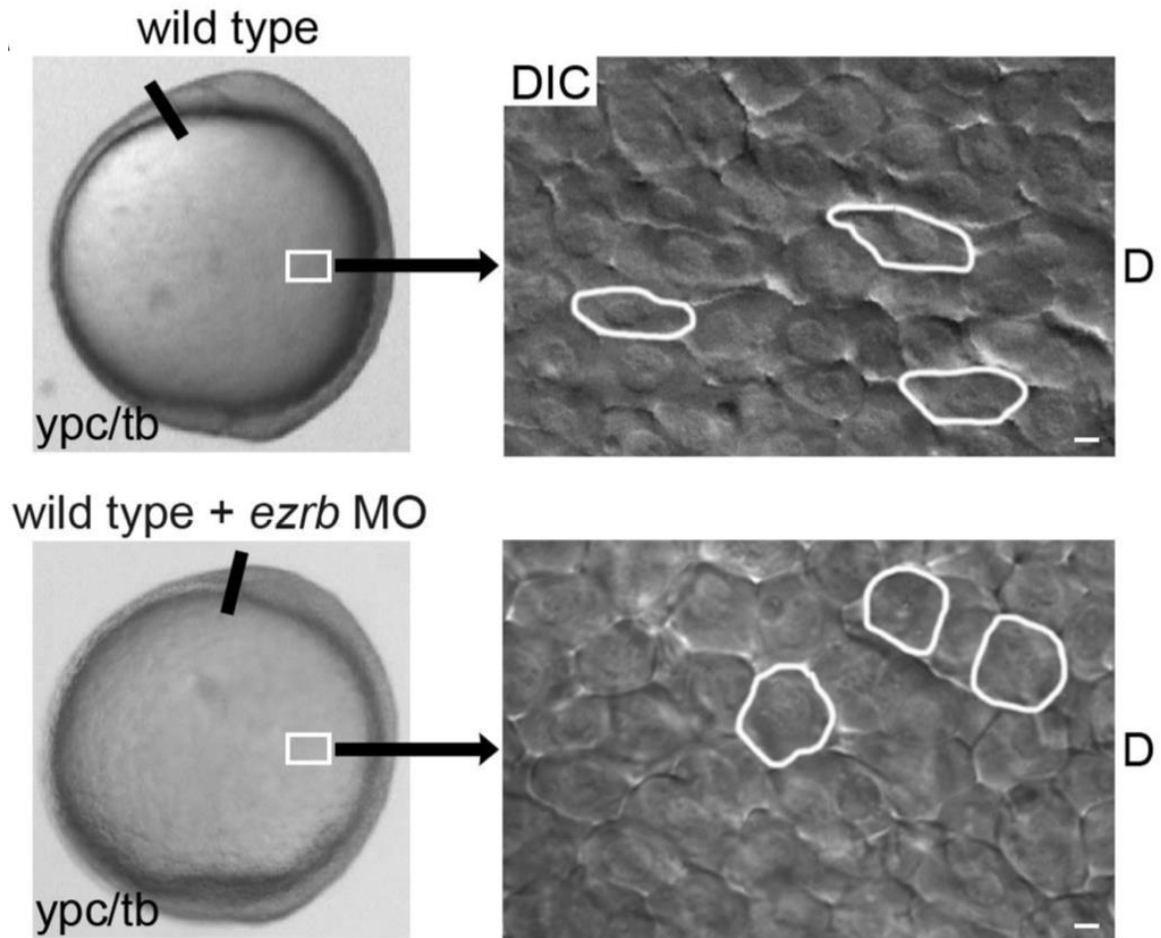


Figure 14. Ezrinb morphants display a C&E phenotype: Whole mount embryo images of wild-type and *ezrb* morphant embryos. White box indicates approximate area of time-lapse imaging. DIC time-lapse images showing mesodermal cells at tailbud stage from wild-type and *ezrb* morphant embryos. Dorsal is to the right and anterior is to the top. Representative cells are outlined in white to show elongation and alignment in relation to the dorsal-ventral axis. D, dorsal. Scale bars, 5 μ m.

Ezrinb function is required for PCP and bleb reduction

To determine the effects of blebbing at late gastrulation, we injected wild-type embryos with a *ezrb* MO at 1-cell stage and cells were analyzed by DIC time-lapse imaging. A significant loss of PCP is seen in *ezrb* morphants by analysis of PCP readouts, cell length-width ratio (LWR) (Figure 15A) and mediolateral alignment (MLA) (Figure 15A,B). LWR is calculated by dividing the length of the cell by the width. MLA represents the percentage of cells aligned mediolaterally. Cells are considered aligned if they are ± 20 degrees in relation to the notochord. Wild-type mesodermal cells have a LWR of 1.59 ± 0.32 with $MLA \pm 20^\circ = 70\%$ compared to *Ezrb* morphants which have a LWR of 1.34 ± 0.20 with $MLA \pm 20^\circ = 46\%$ (Figure 15A,B). We also found the percentage of cells forming blebs is increased in *ezrb* morphant embryos at tailbud stage compared to controls (Figure 15C). However, the number of blebs per cell was unaffected by knocking down *Ezrb* protein levels in wild-type embryos (not shown).

Conversely, we wanted to inhibit bleb protrusions at mid-gastrulation to determine if decreased blebbing can influence mesendodermal cell migration. To do this, a synthetic mRNA construct encoding a constitutively active form of *Ezrb* (*ca-ezrb*; T564D) was injected into wild-type embryos at the one-cell stage, and DIC time-lapse imaging was used to analyze cells at 80% epiboly. We found expression of activated *Ezrb* inhibits bleb formation as the percentage of cells forming blebs was decreased in embryos injected with *ca-ezrb* compared to wild-type 80% epiboly controls (Figure 15A). The number of blebs per cell was significantly decreased by increased *Ezrb* function (not shown). LWR and MLA of mesendodermal cells at mid-gastrulation remained unaffected after *ca-ezrb* injection (Figure 15A,B).

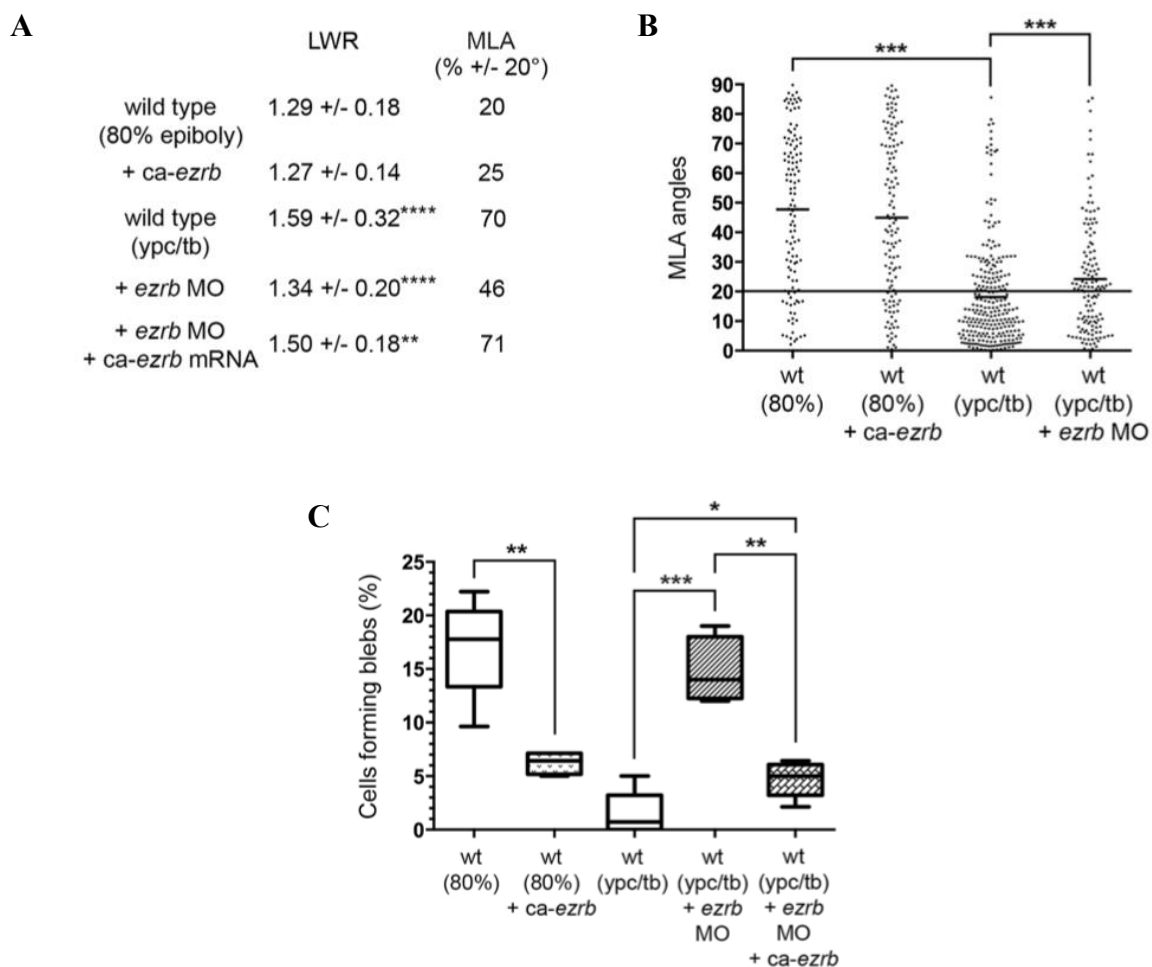


Figure 15. Blebbing at late gastrulation inhibits PCP: (A) LWR and MLA quantification from mesendodermal and mesodermal wild-type and *ezrb* morphant cells (wt 80% epiboly, n=150 cells, 4 embryos; wt 80% epiboly + *ca-ezrb*, n=126 cells, 4 embryos, wt tailbud, n=265 cells, 8 embryos, wt tailbud + *ezrb* MO, n=137 cells, 4 embryos; wt tailbud + *ezrb* MO + *ca-ezrb* mRNA, n=93 cells, 4 embryos). (B) MLA data from panel B shown in degrees as individual data points. Horizontal black line denotes 20 degrees. (C) Percentage of cells forming blebs from mesendodermal and mesodermal wild-type and *ezrb* morphant cells. Analysis is from 15-minute DIC time-lapse videos (wt 80% epiboly + *ca-ezrb* mRNA, n=560 cells, 4 embryos; wt tailbud + *ezrb* MO, n=400 cells, 4 embryos; wt tailbud + *ezrb* MO + *ca-ezrb* mRNA, n=140 cells, 5 embryos). Scatter plot (B) shows individual data points and average values. Box plot (C) displays data as the interquartile dataset, the median, and the data range. * $P < 0.05$, ** $P < 0.01$, *** $P < 0.001$, **** $P < 0.0001$; unpaired Student's t-test with Welch's correction except panel B which is Watson non-parametric two-sample U^2 test.

Ezrinb is required for directed migration

Next, we analyzed cell migration paths using DIC time-lapse imaging and cell tracking software to compare how disrupting bleb protrusive-activity at mid- and late gastrulation affected cell migration trajectories. Directness values were determined by dividing the Euclidean distance by the total accumulated distance and determine how straight a cells path is from starting to end point during a time-lapse video. We found when bleb protrusions were stimulated by *Ezrb* knockdown, tailbud stage mesodermal cells had significantly decreased migration directness (0.63) compared to control cells (0.91) (Figure 16A,B). At 80% epiboly, directness of mesendodermal cells was significantly increased in *ca-ezrb* mRNA injected embryos (0.49) compared to controls (0.41) (Figure 16A,B).

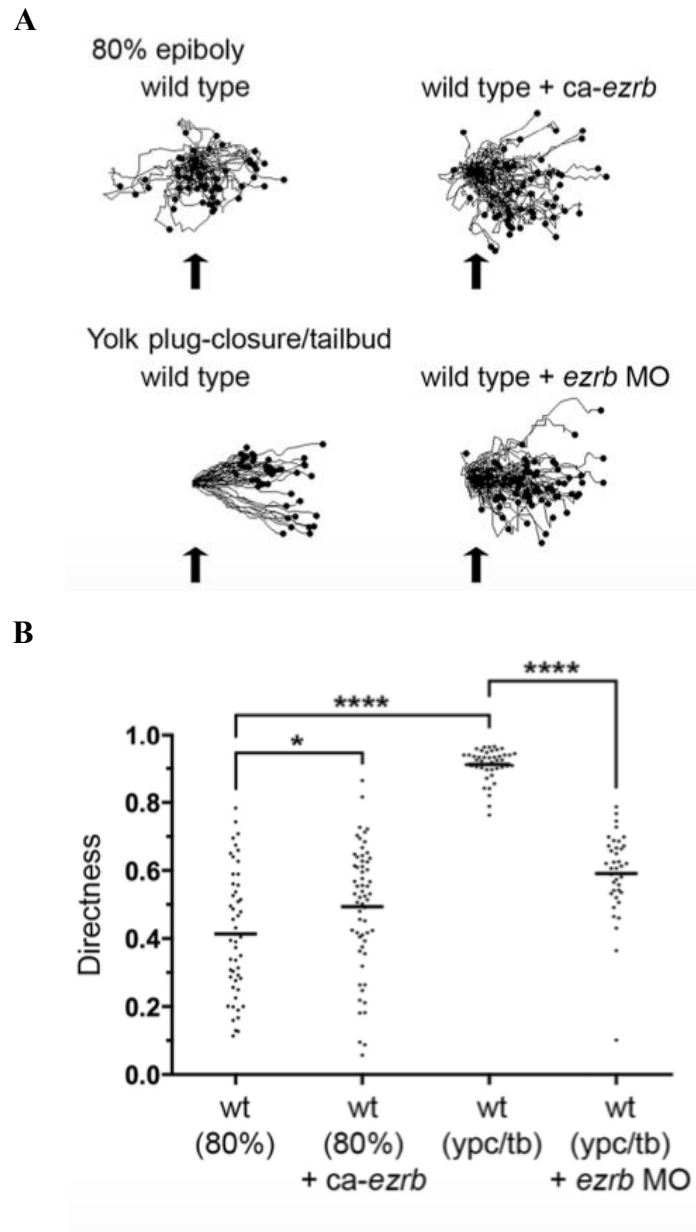


Figure 16. Ezrinb is required for directed migration: (A) Individual cell migration tracks showing dorsal convergence of mesendodermal and mesodermal wild-type and *ezrb* morphant cells. Black arrows show standard point of origin for comparison. (B) Individual wild-type and *ezrb* morphant mesendodermal and mesodermal cell directness values. Scatter plot shows individual data points and average values (wt 80% epiboly, n=50 cells, 3 embryos; wt + *ca-ezrb* 80% epiboly, n=60 cells, 3 embryos; wt tailbud, n=44 cells, 3 embryos; wt + *ezrb* MO, n=77 cells, 3 embryos). * $P < 0.05$, **** $P < 0.0001$; unpaired Student's t-test with Welch's correction.

***ezrinb* MO injected embryos have mediolaterally broadened mesoderm**

By western blot, Ezrb protein levels were quantified in wild-type embryos injected with the *ezrb* MO to confirm protein knockdown (Figure 17). To confirm our MO did not present off-targeted effects, we co-injected embryos with both MO and the activated form of Ezrb. We show co-injection of *ezrb* MO and *ca-ezrb* successfully rescued the bleb and PCP phenotype in *ezrb* morphants to approximate wild-type levels (wt, LWR of 1.59 ± 0.32 , MLA $\pm 20^\circ=70\%$; wt + *ezrb* MO, LWR of 1.34 ± 0.20 , MLA $\pm 20^\circ=46\%$; wt + *ezrb* MO + *ezrb* mRNA, LWR of 1.50 ± 0.18 , MLA $\pm 20^\circ=71\%$, 5.36% of cells forming blebs). To confirm the C&E phenotype was due to defective mesodermal cell movements and not notochord disorders, whole mount *in situ* hybridization (WISH) was performed and genetic marker, *protocadherin 8* (*pcdh8*), was used to mark the width of the paraxial/lateral mesoderm. When measured, we found *ezrb* morphant paraxial/lateral mesoderm is approximately 10% wider than wild-type controls confirming *ezrb* morphant defects are due to failure of dorsal convergence movements and not notochord defects (Figure 18).



Figure 17. Western blot showing Ezrinb knockdown: Western blot showing knockdown of Ezrb from total protein extracts of wild-type embryos injected with a *ezrb* MO at tailbud stage. This was performed in triplicate. Band density values are shown beneath each lane.

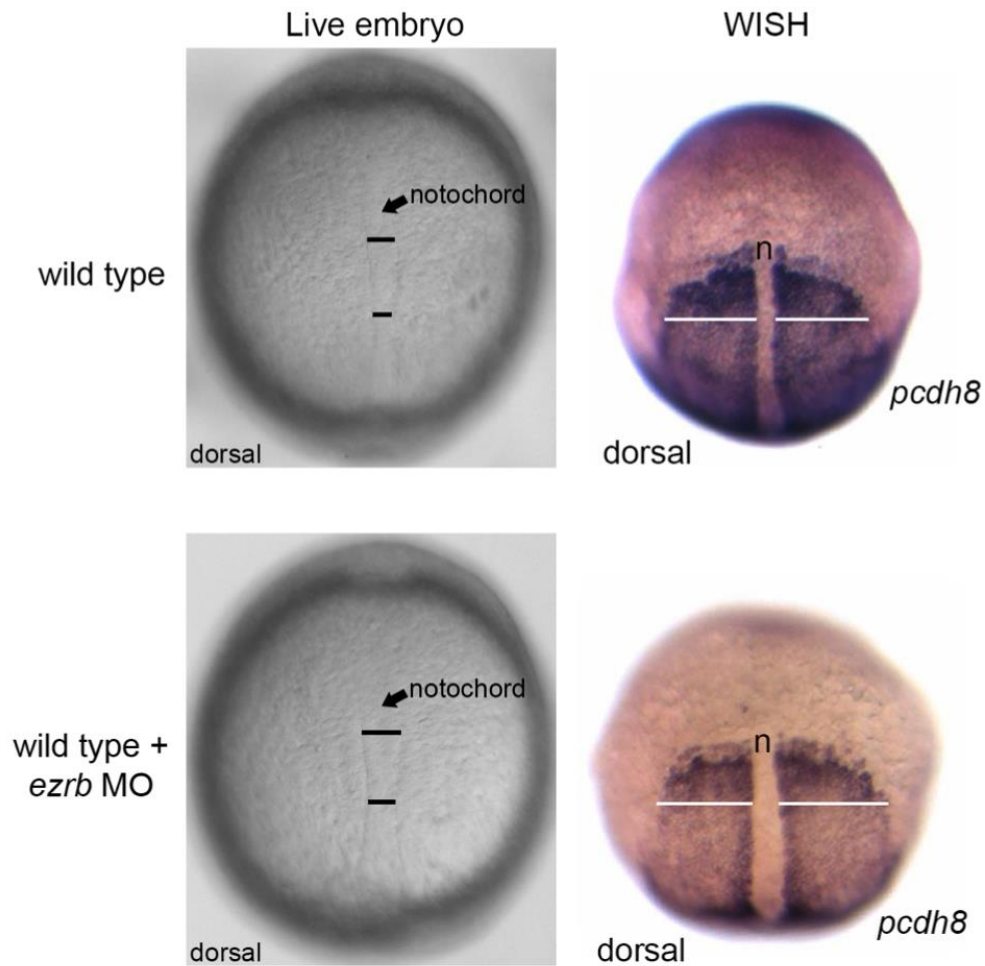


Figure 18. *ezrinb* morphant embryos have mediolaterally broadened mesoderm: Brightfield microscopy live and whole-mount in situ hybridization (WISH) images of wild-type and *ezrb* morphant embryos at tailbud stage. Shown are dorsal views with anterior to the top. Notochord is denoted by black arrow and the notochord widths by black lines (live embryo images). White lines indicate the width of *protocadherin 8* (*pcdh8*) staining showing paraxial/lateral mesoderm. Paraxial/lateral mesoderm in *ezrb* morphants is approximately 10% wider than in control embryos. n, notochord.

4.3 Conclusion

Thus far we have shown blebs are suppressed by late gastrulation when actin-based protrusions seem to be more efficient. This suppression of bleb protrusions observed from mid- to late gastrulation suggests blebbing at later stages is inhibitory for processes occurring during this developmental period. Therefore, in this chapter, we aimed to alter bleb activity at mid- and late gastrulation using an *ezrb* morpholino and a *ca-ezrb* construct.

We found *ezrb* morphant embryos displayed a slight C&E phenotype characterized by a shortened and broadened body axis, which is suggestive of defective LWR and MLA. We found increased blebbing by Ezrinb knockdown at late gastrulation hindered PCP by decreasing LWR and MLA of mesodermal gastrula cells. This suggests Ezrb function is necessary for establishment of PCP. In addition, it was also observed that Ezrb is required for directed migration of mesodermal gastrula cells as directness was decreased compared to controls. These data show that the protrusive activity of blebs is inhibitory to PCP establishment and directed migration. By contrast, we reasoned that inhibition of bleb protrusions at mid-gastrulation could promote PCP or directed migration of mesodermal cells. Indeed, we found injection *ca-ezrb* mRNA was sufficient to reduce blebbing and increase directness at 80% epiboly but had no effects on LWR or MLA. We attribute this to a shift from bleb to actin-based protrusions preventing cells from entering tumbling phases and an increase in cell packing (Diz-Muñoz et al., 2016).

In summary, these data show that expression of activated Ezrb decreased the formation of bleb protrusions at 80% epiboly, while Ezrb knockdown increased bleb protrusions at tailbud stage. This data suggests that there are mechanisms to inhibit blebbing in mesodermal cells, and these mechanisms likely involve Ezrb protein activation.

CHAPTER FIVE. Role of Adhesive Proteins for Bleb Suppression at Late Gastrulation.

5.1 Introduction

During zebrafish gastrulation, mesendodermal cells lack PCP and display meandering trajectories, reduced cell-cell contacts and decreased cohesion (Jessen et al., 2002). By late gastrulation stage, cells display PCP-dependent polarity as demonstrated by higher LWR's and MLA (Jessen et al., 2002, Topczewski et al., 2001). Correlating with this change in cell morphology is an increase in a fibronectin ECM and cell surface expression of the cell-cell adhesion protein Cdh2. At mid-gastrulation there is a single, minute layer of fibronectin that is located between the epiblast and hypoblast germ layers (Latimer and Jessen, 2010). This means the deepest layer of mesendodermal cells is not in contact with a fibronectin ECM. By late gastrulation, two layers of fibronectin, one beneath the ectoderm and one between the mesoderm and endoderm, are found (Latimer and Jessen, 2010). Previous studies showed ECM density can influence directed migration and membrane-protrusive activity (Charras and Sahai, 2014).

As cells undergo collective migration, a coordination between cell-cell and cell-ECM contacts is required (Friedl and Gilmour, 2009; Mishra et al., 2019). In zebrafish, Cdh2 is highly expressed in mesodermal gastrula cells (Harrington et al., 2007; Warga and Kane, 2007). Moreover, we show Cdh2 expression at the cell surface increases from mid- to late gastrulation, as shown by fluorescence confocal microscopy (Figure 21). Cell culture studies have indicated migrating cells are capable of modifying protrusive activity based on ECM structure and adhesiveness. Based on these data, we hypothesize proper

levels of the adhesive proteins, fibronectin and Cdh2, are necessary for PCP and directed migration of mesodermal gastrula cells.

5.2 Results

Mesodermal cell surface expression of Cdh2 increases from mid- to late gastrulation

To determine Cdh2 expression patterns of mesendodermal/mesodermal cells from mid- to late gastrulation, we used immunohistochemistry to label Cdh2 with a pan-cadherin antibody. This antibody labels both Cdh1 and Cdh2; however, Cdh1 is only expressed in the ectoderm of the embryo. We confirmed pan-cadherin labeling of only Cdh2 by injection of *cdh2* MO, which showed diminished expression of pan-cadherin staining at 80% epiboly. Ultimately, we found plasma membrane Cdh2 expression is significantly higher in tailbud stage embryos compared with 80% epiboly (Figure 19A). Cell membrane fluorescence intensity was quantified (Figure 19B).

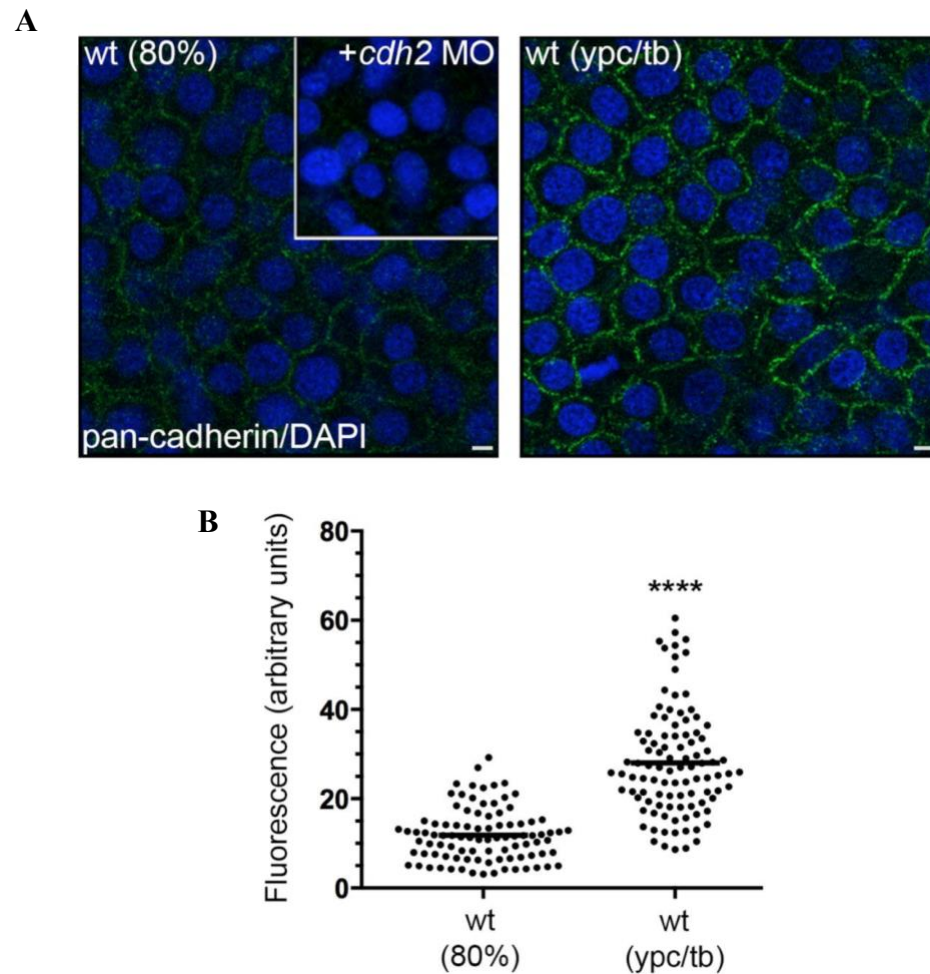


Figure 19. Cell surface *cdh2* expression increases from mid- to late gastrulation: (A) Pan-cadherin (green) and DAPI (blue) immunofluorescent labeling of wild-type mesendodermal and mesodermal cells. Inset image shows pan-cadherin/DAPI staining in *cdh2* morphant mesendodermal cells. Scale bars: 5 μ m. **(B)** Fluorescence intensity quantified per cell showing significant increase in fluorescence at tailbud stage. Scatter plot shows individual data points and average values. **** P <0.0001; unpaired Student's *t*-test with Welch's correction.

Fibronectin and Cdh2 are required for PCP

Antisense MOs were used to analyze the function of the adhesive proteins, fibronectin and Cdh2. For fibronectin, a combination of MOs were used to knockdown the protein levels of both fibronectin genes (*fn1a* and *fn1b*) (Jülich et al, 2005; Latimer and Jessen, 2010; Love et al., 2018), and for Cdh2, a MO that binds the *cdh2* 5' untranslated region (UTR) that mimics defects of homozygous/null mutant embryos (Lele et al., 2002). We found that late gastrulation stage *fn1a/1b* and *cdh2* morphants exhibited a slight C&E phenotype usually indicative of a PCP defect (Figure 20A). Indeed, compared to wild-type mesodermal cells, *fn1a/1b* and *cdh2* morphant mesodermal cells had reduced LWR's and MLA indicative of defective PCP (wt, LWR=1.59 ± 0.32, MLA±20°=71%; wt + *fn1a/1b* MO, LWR=1.34±0.19, MLA±20°=59%; wt + *cdh2* MO, LWR=1.31±0.19, MLA±20°=36%) (Figure 20B,C). By contrast, we reasoned that expression of *fn1a/1b* mRNA at 80% epiboly when there is little fibronectin ECM will have effects on cell LWR and MLA. We found overexpression of *fibronectin* mRNA at mid-gastrulation was sufficient to promote MLA but not LWR (wt 80%, LWR=1.29±0.18, MLA±20°= 20%; wt 80% + *fn1a/1b* mRNA, LWR=1.32± 0.20, MLA±20°=34%) (Figure 20B,C).

Next, to verify the *fn1a/1b* and *cdh2* MO did not have off target effects, wild-type embryos were co-injected with *fn1a/1b* MO and mRNA or *cdh2* MO and mRNA. We found LWR and MLA values were rescued to levels similar to controls (wt, LWR = 1.59 ± 0.32, MLA ± 20° = 71%; wt + *fn1a/1b* MO, LWR = 1.34 ± 0.19, MLA ± 20°= 59%; wt + *fn1a/1b* MO + *fn1a/1b* mRNA, LWR = 1.57 ± 0.26, MLA ± 20°= 66%; wt + *cdh2* MO, LWR = 1.31 ± 0.19, MLA ± 20° = 36%; wt + *cdh2* MO + *cdh2* mRNA, LWR = 1.59 ± 0.29, MLA ± 20° = 63% (Figure 20B).

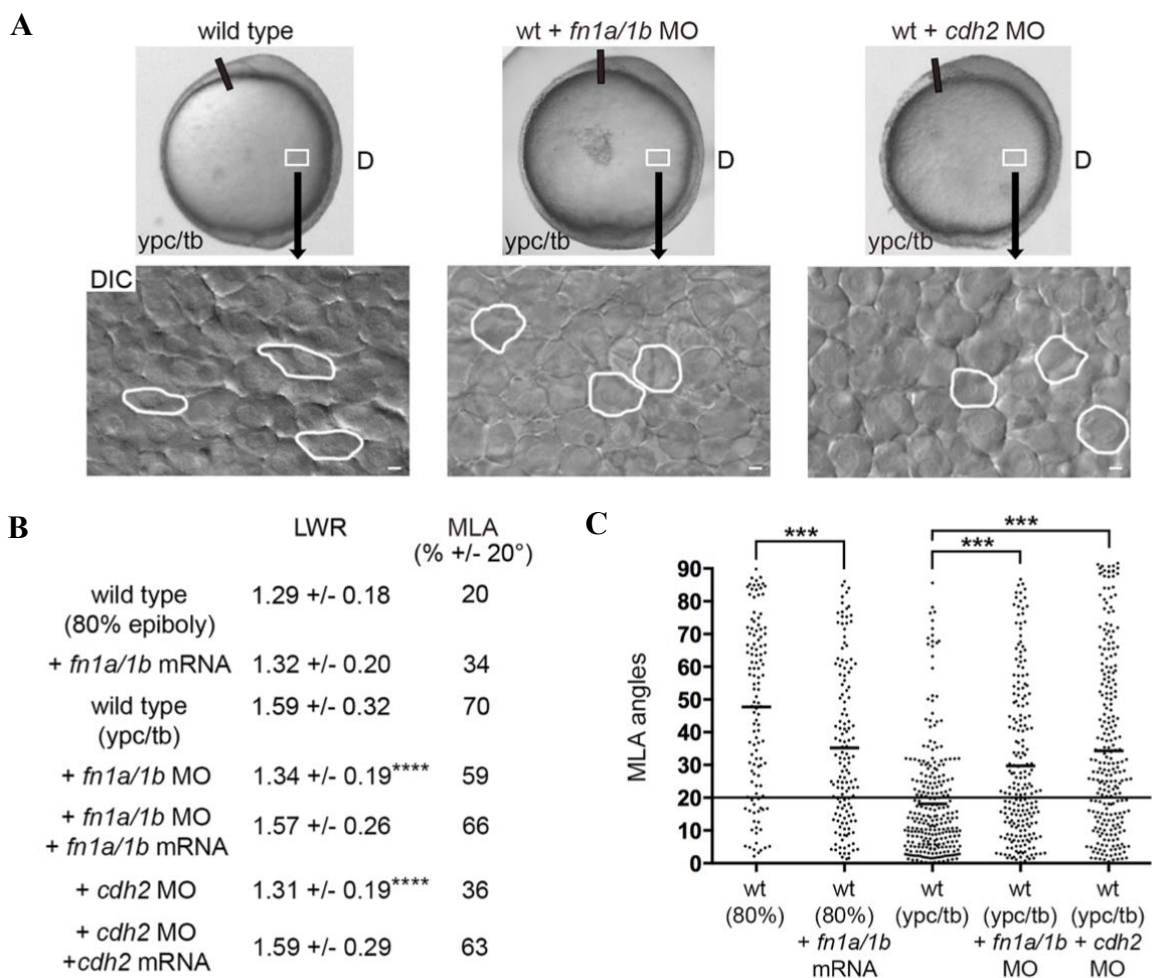


Figure 20. Fibronectin and Cdh2 facilitate proper PCP: (A) Live whole mount lateral embryo images and cellular DIC time-lapse images of wild-type control and *fibronectin* and *cdh2* morphant embryos. White boxes represent approximate area of imaging. Cells outlined in white show elongation and alignment. Dorsal is to the right and anterior is to the top. D, dorsal. Scale bars: 5 μ m. (B) LWR and MLA quantification of wild-type control and *fibronectin* and *cdh2* morphant mesodermal cells (wt 80% epiboly+*fn1a/1b* mRNA, n=140 cells, 5 embryos; wt tailbud+*fn1a/1b* MO, n=211 cells, 5 embryos; wt tailbud+*fn1a/1b* MO+*fn1a/1b* mRNA, n=73 cells, 4 embryos; wt tailbud+*cdh2* MO, n=238 cells, 4 embryos; wt tailbud+*cdh2* MO+*cdh2* mRNA, n= 60 cells, 3 embryos). (C) MLA data from panel B shown in degrees as individual data points. Horizontal black line denotes 20 degrees. Scatter plots show individual data points and average values. *** P <0.001, **** P <0.0001; unpaired Student's t -test with Welch's correction except C which is Watson non-parametric two-sample U_2 test.

Fibronectin and Cdh2 function to suppress blebbing at late gastrulation

To analyze a possible relationship between adhesion proteins, fibronectin and Cdh2, and the formation of bleb protrusions, DIC time-lapse videos of *fn1a/1b* and *cdh2* morphants were analyzed and bleb protrusions counted. Our data show a higher percentage of mesodermal cells formed bleb protrusions in *fn1a/1b* (22.5%) and *cdh2* (24.52%) morphant embryos compared with wild-type controls (1.43%) (Figure 21A). Validation experiments for both *fn1a/1b* and *cdh2* MO's were performed, and showed successful rescue of the percentage of cells forming blebs back to percentages comparable to wild type (wt = 1.43%; wt + *fn1a/1b* MO + *fn1a/1b* mRNA = 4.46%; wt + *cdh2* MO + *cdh2* mRNA = 3.75%) (Figure 21A).

Next, we questioned whether *fibronectin* mRNA expression at mid-gastrulation would suppress bleb protrusion formation and influence directed migration. We found the percentage of mesendodermal cells with blebs at 80% epiboly was reduced in *fn1a/1b* mRNA-injected wild-type embryos compared with controls embryos (wt 80% = 17.037%; wt 80% + *fn1a/1b* mRNA = 6.607%) (Figure 21B).

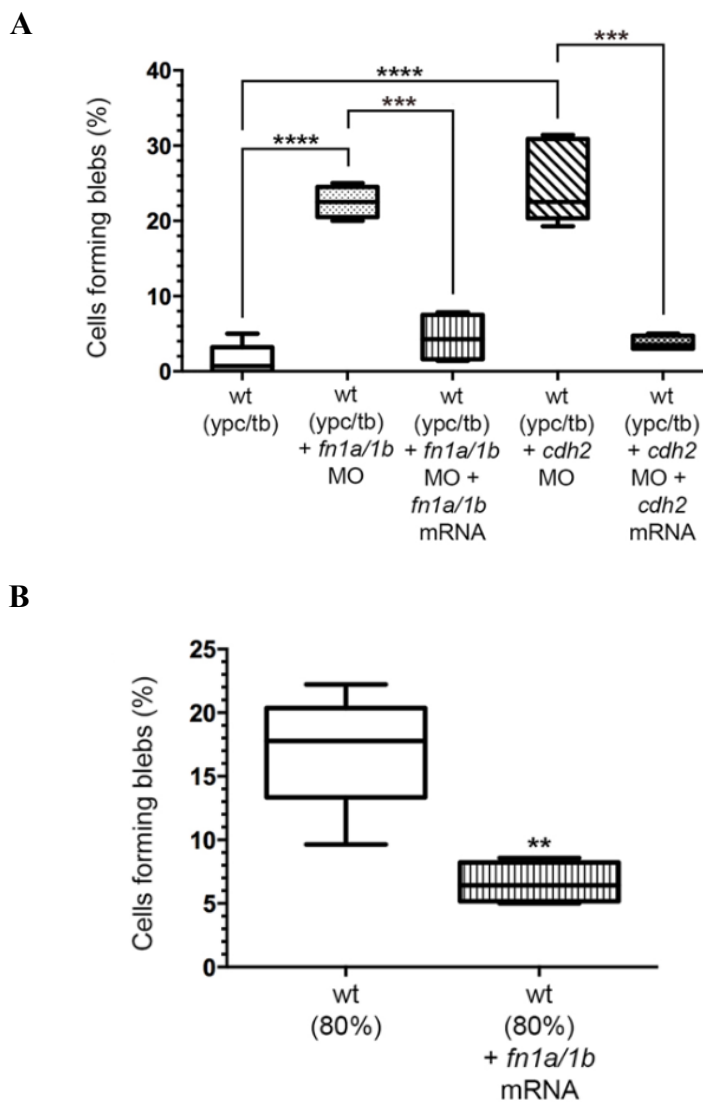


Figure 21. Fibronectin and Cdh2 are required for proper bleb protrusive activity: (A) Percentage of mesodermal cells forming blebs in wild-type control, *fibronectin*, and *cdh2* morphant embryos. Analysis is from 15-minute DIC time-lapse videos (wt tailbud+*fn1a/1b* MO, n=400 cells, 4 embryos; wt tailbud+*fn1a/1b* MO+*fn1a/1b* mRNA, n=140 cells 4 embryos; wt tailbud+*cdh2* MO, n=840 cells, 6 embryos; wt tailbud+*cdh2* MO+*cdh2* mRNA, n=400 cells, 4 embryos). **(B)** Percentage of mesendodermal cells forming blebs in wild-type control and *fibronectin* morphant embryos (wt 80% epiboly+*fn1a/1b* mRNA, n=560 cells, 4 embryos). Box plots displays data as the interquartile dataset, the median, and the data range. ** $P < 0.01$, *** $P < 0.001$, **** $P < 0.0001$; unpaired Student's *t*-test with Welch's correction.

To determine if *fn1a/1b* or *cdh2* morphants had defective directed migration, we performed individual cell tracking using FIJI software and DIC time-lapse videos. We found both *fn1a/1b* and *cdh2* morphant mesodermal cells had significantly decreased directness compared with wild-type mesodermal cells (wt = 0.91; wt + *fn1a/1b* MO = 0.57; wt + *cdh2* MO = 0.59) (Figure 22A,B). Notably, the directness values of mesendodermal cells in *fn1a/1b* mRNA-injected embryos showed a significantly higher value compared to controls (wt 80% = 0.41; wt + *fn1a/1b* mRNA = 0.50) (Figure 22B).

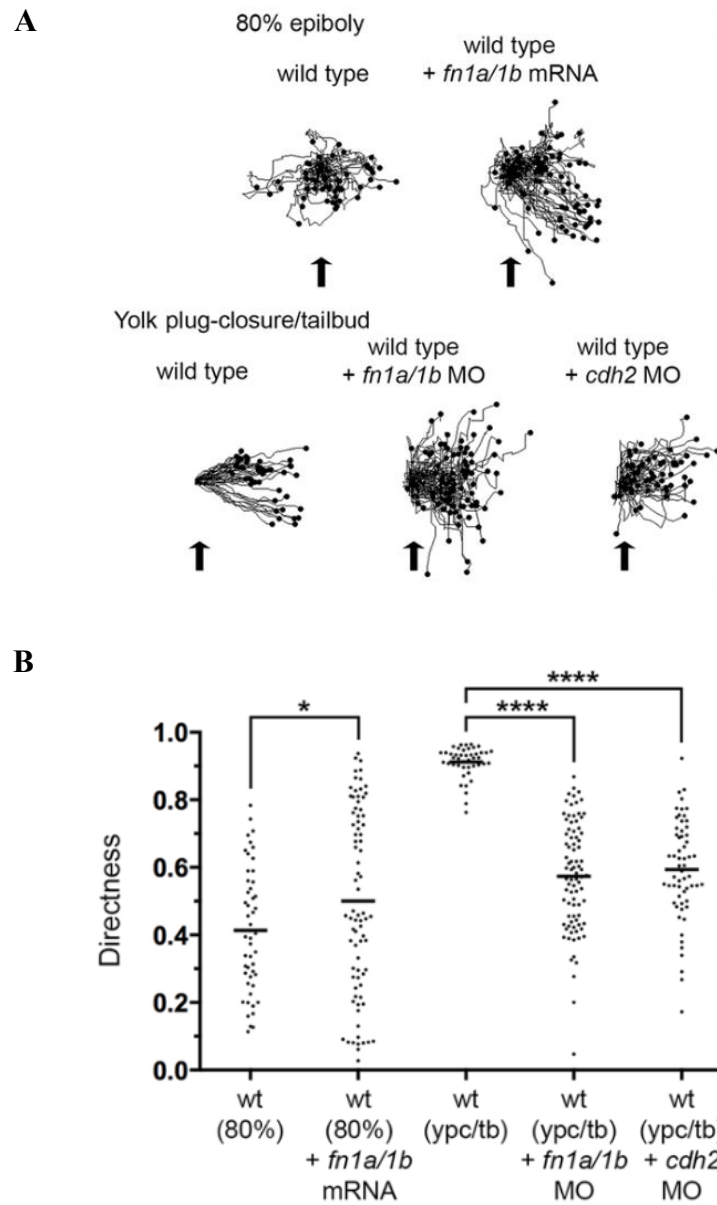


Figure 22. Fibronectin and Cdh2 support directed migration: (A) Individual cell migration tracks showing dorsal convergence of mesendodermal and mesodermal wild-type controls and *fibronectin* and *cdh2* morphant cells. Black arrows show standard point of origin for comparison (wt+*fn1a/1b* mRNA, n=80 cells, 3 embryos; wt+*fn1a/1b* MO, n=86 cells, 3 embryos; wt+*cdh2* MO, n=60 cells, 3 embryos). (B) Individual mesendodermal and mesodermal cell directness values. Scatter plot shows individual data points and average values. * $P < 0.05$, **** $P < 0.0001$; unpaired Student's *t*-test with Welch's correction.

cdh2^{tm101/tm101} mutants phenocopy *cdh2* morphant phenotypes

To confirm protein knockdown, western blot analysis was performed on total protein extracts that were generated from wild-type embryos injected with a *cdh2* MO to confirm protein knockdown. A pan-cadherin antibody was used to probe the blot for Cdh2. Pan-cadherin recognizes Cdh1 and Cdh2 during zebrafish gastrulation. We show our MO was successful at knocking down Cdh2 protein levels (Figure 23).

The *cdh2* mutants were additionally imaged by DIC microscopy and analyzed to confirm results by MO. To do this, twelve embryos from a *cdh2^{tm101/+}* incross were selected randomly and DIC time-lapse imaging was performed (5 minutes with 30 second sampling intervals). Because *cdh2^{tm101/tm101}* mutants do not show a phenotype, to identify mutants, each embryo was genotyped. Genomic DNA was generated in embryos, PCR amplified, and sequenced (Figure 26B). Homozygous *cdh2^{tm101/tm101}* embryos have a missense mutation of Threonine to Alanine at amino acid Tyrosine 514 which introduces a stop codon (Lele et al., 2002) (Figure 24A). We confirmed our MO findings and showed that the percentage of cells forming blebs in our *cdh2^{tm101/tm101}* mutants was 11% compared to 1% in *cdh2* siblings. The PCP phenotype was also observed in *cdh2^{tm101/tm101}* mutants (*cdh2* sibling, LWR = 1.49 ± 0.25 , MLA $\pm 20^\circ$ = 72%; *cdh2^{tm101/tm101}*, LWR = 1.23 ± 0.15 , MLA $\pm 20^\circ$ = 38%) (Figure 24C).

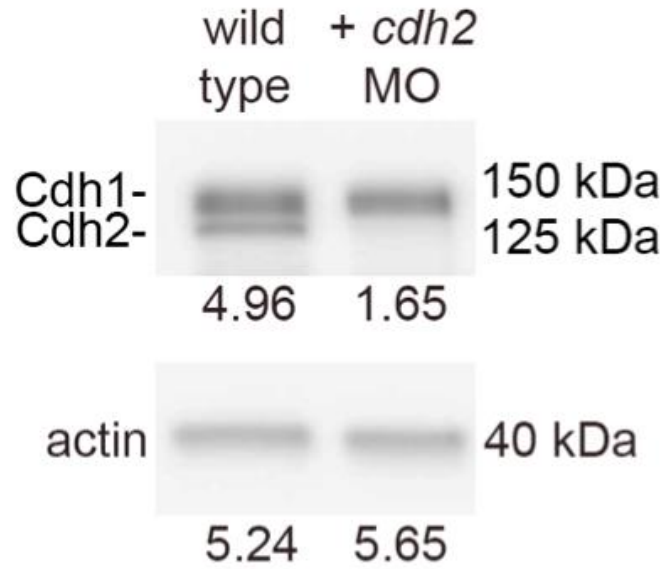


Figure 23. Western blot showing Cdh2 knockdown: Western blot showing knockdown of Cdh2 from total protein extracts of wild-type embryos injected with a *cdh2* MO from tailbud stage. Blots were re-probed with β -actin antibody. Relative densitometry are shown beneath each lane.

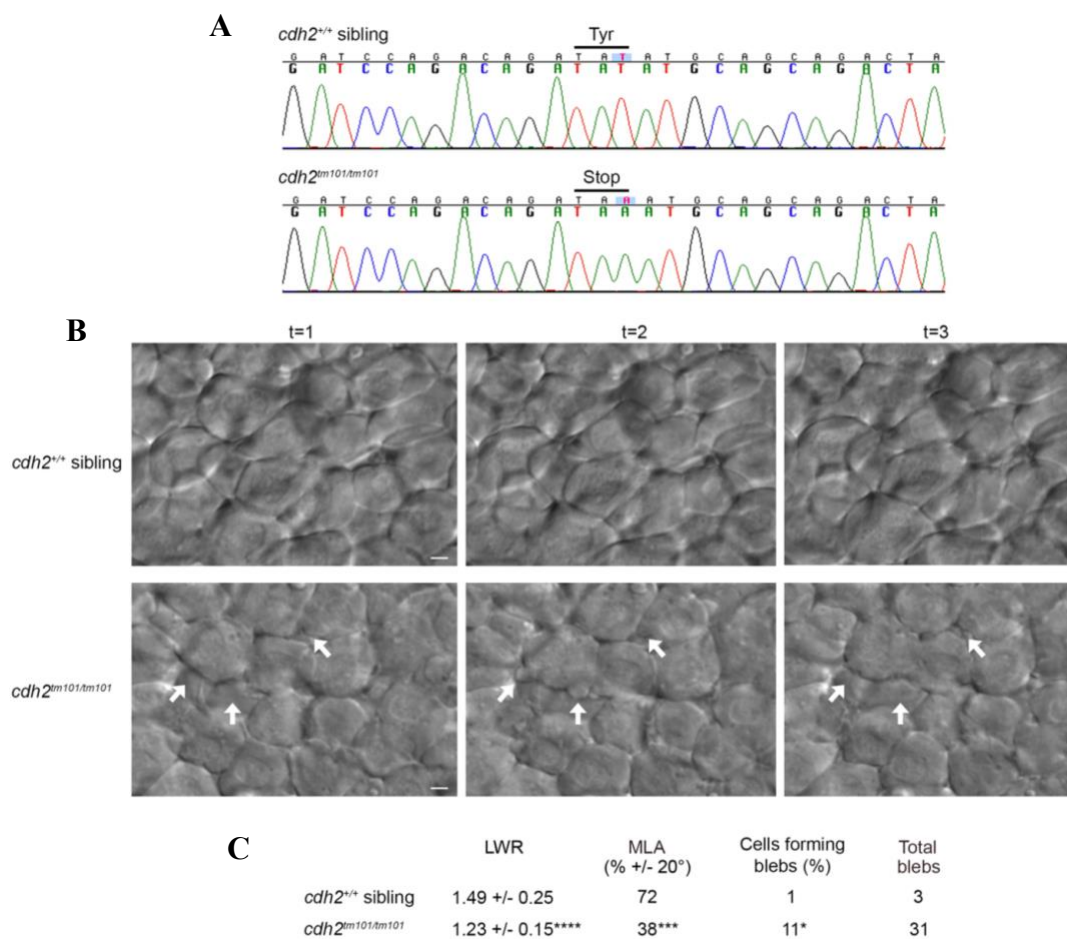


Figure 24. Homozygous *cdh2tm101/tm101* mutant embryos phenocopy *cdh2* morphants: (A) DIC time-lapse imaging (5 minutes with 30 second imaging intervals) was performed on twelve randomly selected embryos from a *cdh2tm101/tm101* incross and subjected to genotyping using PCR amplification of genomic DNA. Images shown are 1, 2, and 3 minute. Homozygous *cdh2tm101/tm101* embryos were identified by the introduction of a stop codon resulting from a base pair change from T to A at amino acid Tyr 514 (Lele et al., 2002). (B) DIC time-lapse images of *cdh2*^{+/+} sibling and *cdh2tm101/tm101*. White arrows denote blebs forming in homozygous mutants. (C) Confirmed homozygous *cdh2tm101/tm101* embryos displayed defective PCP and increased mesodermal cell blebbing compared to *cdh2*^{+/+} sibling. (*cdh2*^{+/+} siblings and *cdh2tm101/tm101* mutants, n=50 cells for PCP analysis, n=280 cells for bleb analysis, 2 embryos per genotype). *** $P < 0.001$, **** $P < 0.0001$; unpaired Student's *t*-test with Welch's correction.

5.3 Conclusion

In this chapter, we aimed to determine the role of fibronectin and Cdh2 for PCP establishment, directed migration, and protrusion formation. We found that mesodermal cells in *fibronectin* morphants had decreased LWR, MLA, and directed migration. In addition, our data showed fibronectin knockdown at late gastrulation stimulated an increase in the percentage of cells forming blebs. Therefore, we suggest fibronectin is required for PCP establishment and bleb suppression at late gastrulation. Additionally, we found that injection of *fibronectin* mRNA promoted the MLA and directed migration of mesodermal cells at mid-gastrulation. This data collectively suggests that the increase in a fibronectin ECM from mid- to late gastrulation is required for PCP establishment, directed migration, and a shift in protrusive activity.

Next, we found an increase in Cdh2 cell surface expression at late gastrulation. Like fibronectin, we aimed to determine the requirement of Cdh2 for PCP establishment, directed migration, and protrusion formation. We found that PCP was inhibited in mesodermal cells when Cdh2 protein levels were knocked down. Our data also show that in addition to fibronectin, Cdh2 functions to suppress bleb protrusions in mesodermal cells at late gastrulation but not ectodermal cells. Cdh2 knockdown in lateral ectodermal cells did not disrupt PCP defects or stimulate bleb formation (WT, LWR=1.63, $MLA \pm 20^\circ = 86\%$, n=151 cells, 3 embryos; WT+*cdh2* MO, LWR=1.58, $MLA \pm 20^\circ = 84\%$, n=141 cells, 3 embryos). Taken together, these data suggest fibronectin and Cdh2 are necessary for bleb suppression and PCP at late gastrulation, and we suggest that increased fibrillar fibronectin ECM at late gastrulation influences a transition from bleb-based to actin-based protrusions.

CHAPTER SIX. *Vangl2* is Required for Bleb Suppression at Late Gastrulation, and Functions Cell-Autonomously to Regulate Protrusions

6.1 Introduction

At late gastrulation, *vangl2* mutant mesodermal cells look like mid-gastrulation stage wild-type mesodermal cells because they fail to transition to polarized cell behaviors. Instead, they maintain a round cell shape, fail to align along the mediolateral axis, exhibit decreased cohesion, and undergo indirect migration to the dorsal axis (Jessen et al., 2002). Thus far, data from this study suggests there is a correlation between bleb protrusion formation and disrupted PCP in late gastrulation stage mesodermal cells. Therefore, in this section we aimed to characterize bleb protrusive activity in the mesoderm of *vangl2* mutant embryos. We hypothesized that mesodermal cells of *vangl2* mutant embryos have improper bleb protrusive activity. Furthermore, based on defects in *vangl2* mutants, we also aimed to determine the effects of *fibronectin* mRNA and *ca-ezrb* expression in *vangl2* mutant mesodermal cells. Due to decreased protein levels of fibronectin in *vangl2* mutant embryos, we hypothesized *fibronectin* mRNA expression could potentially rescue cellular phenotypes. Also, if *vangl2* mutant mesodermal cells have increased bleb protrusions, *ca-ezrb* expression could inhibit blebbing.

Previously published data from early gastrulation stages showed mesodermal cells undergoing directed migration toward the animal pole used actin-based protrusions for runs and blebs during tumbling phases of cell movement (Diz-Muñoz et al., 2016). Here, we hypothesized the balance between blebbing and actin-based protrusion formation is regulated by Ezrin. Furthermore, it has been proposed that blebs can be used during phases of cell reorientation during cell migration.

Blebs differ from actin-based protrusions because they form as a result of actomyosin contractility and hydrostatic pressure as opposed to actin polymerization. Increased actomyosin contractility is thought to increase intracellular pressure resulting in localized separation of the plasma membrane from cortical actin (Fackler and Grosse, 2008). Additionally, as opposed to actin-based protrusions, bleb protrusions do not appear to require integrin-mediated ECM interactions during cell migration (Diz-Muñoz et al., 2010).

How Vangl2 regulates membrane-protrusive activity? In this chapter, we also aimed to determine how Vangl2 regulates blebbing and filopodia in lateral mesodermal cells. It is already established that like other core PCP genes that encode transmembrane proteins, *vangl2* regulates cell elongation and MLA both cell-autonomously and non-autonomously during zebrafish gastrulation (Jessen et al., 2002). This means when *vangl2* mutant cells are transplanted into wild-type backgrounds, *vangl2* disrupted PCP in wild-type cells.

For comparison, we also analyzed how fibronectin regulates protrusion formation also. For these experiments a series of cell transplantation experiments were performed to determine if regulation is cell autonomous or non-autonomous. Cell autonomy describes the cell with the mutation displaying the phenotype of interest. Non-autonomy describes the neighboring cells exhibiting the mutant cells phenotype meaning the mutant cell disrupted the neighboring cells to cause its phenotype.

6.2 Results

Inhibition of blebbing in *vangl2* mutant mesodermal cells rescues MLA and directed migration

To examine the correlation between bleb formation and disrupted PCP, we wanted to analyze blebbing in *vangl2* mutant embryos and manipulate bleb protrusion formation using *fn1a/1b* mRNA and *ca-ezrb*. First, we confirmed *vangl2^{vu67/vu67}* mutants had a PCP phenotype. PCP was measured by calculating LWR and MLA from DIC time-lapse images. We confirmed *vangl2^{vu67/vu67}* had decreased LWR and MLA compared to wild-type mesodermal cells. Wild-type mesodermal cells at tailbud stage had a cellular LWR of 1.59 and the MLA $\pm 20^\circ=70\%$. At the same stage, the cellular LWR of *vangl2^{vu67/vu67}* mutant mesodermal cells was decreased to 1.31 and the percentage of MLA cells was decreased to 42% (Figure 25A,B). Because our work demonstrated that fibronectin is a suppressor of bleb protrusions and influences directed migration of mesodermal cells, we analyzed whether manipulation of *Ezrb* and fibronectin affected *vangl2* mutant phenotypes. We found that at the cellular level injection of *ca-ezrb* mRNA partially rescued MLA but did not rescue LWR. Overexpression of *fn1a/1b* mRNA also did not affect LWR but did partially rescue MLA (Figure 25B,C).

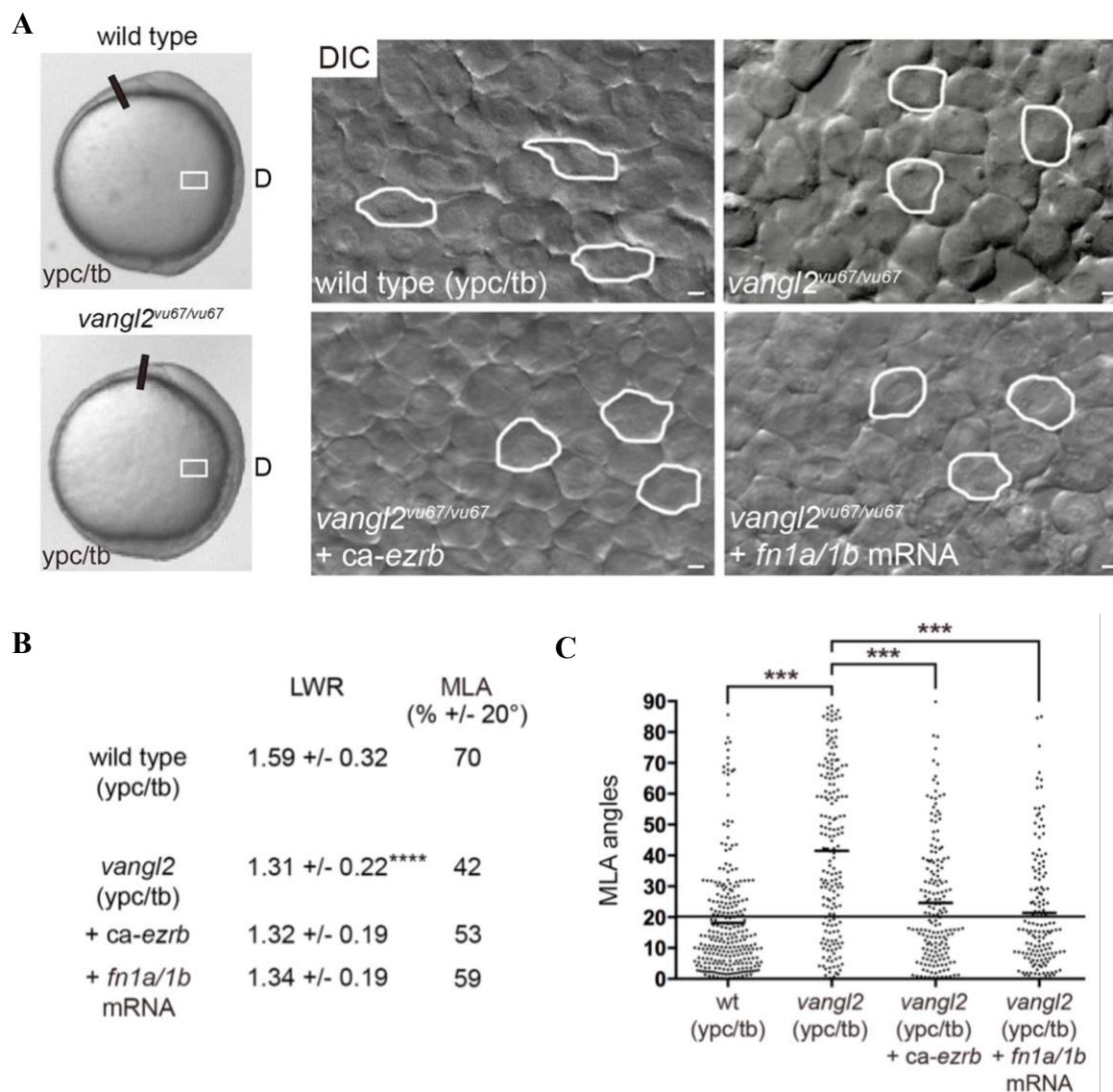


Figure 25. PCP phenotype of *vangl2* mutant mesodermal cells. (A) Live whole mount lateral embryo images of wild-type and *vangl2* mutant embryos. Cellular DIC time-lapse images of wild-type control, *vangl2* mutant and *vangl2* mutant embryos injected with *ca-ezrb* and *fn1a/1b* mRNA (15 minute duration, 30 second intervals). White boxes represent approximate area of imaging. Dorsal is to the right and anterior is to the top. Cells outlined in white show elongation and alignment. D, dorsal. Scale bars: 5 μ m. (B) LWR and MLA quantification of wild-type and *vangl2* mutant mesodermal cells (*vangl2*^{vu67/vu67}, n=180 cells, 4 embryos; *vangl2*^{vu67/vu67}+*ca-ezrb*, n=175 cells, 4 embryos; *vangl2*^{vu67/vu67}+*fn1a/1b* mRNA, n=150 cells, 3 embryos). (C) MLA data shown in degrees as individual data points. Horizontal black line denotes 20 degrees. Scatter plot shows individual data points and average values. *** P <0.001, **** P <0.001; unpaired Student's *t*-test with Welch's correction except C which is Watson non-parametric two-sample U_2 test. Ypc/tb, yolk-plug closure/tailbud stage.

Loss of Vangl2 causes increased bleb protrusion formation

To quantify bleb protrusions, 15-minute DIC time-lapse images were analyzed and bleb protrusions were quantified. We found an increase in the percentage of mesodermal cells forming blebs in *vangl2^{vu67/vu67}* mutant embryos (22.86%) compared to wild-type control mesodermal cells (1.43%) (Figure 26A). However, the percentage of cells forming bleb protrusions was decreased when *vangl2* mutant embryos were injected with either *cazrb* (6.43%) or *fn1a/1b* (13.036%) mRNA (Figure 26B).

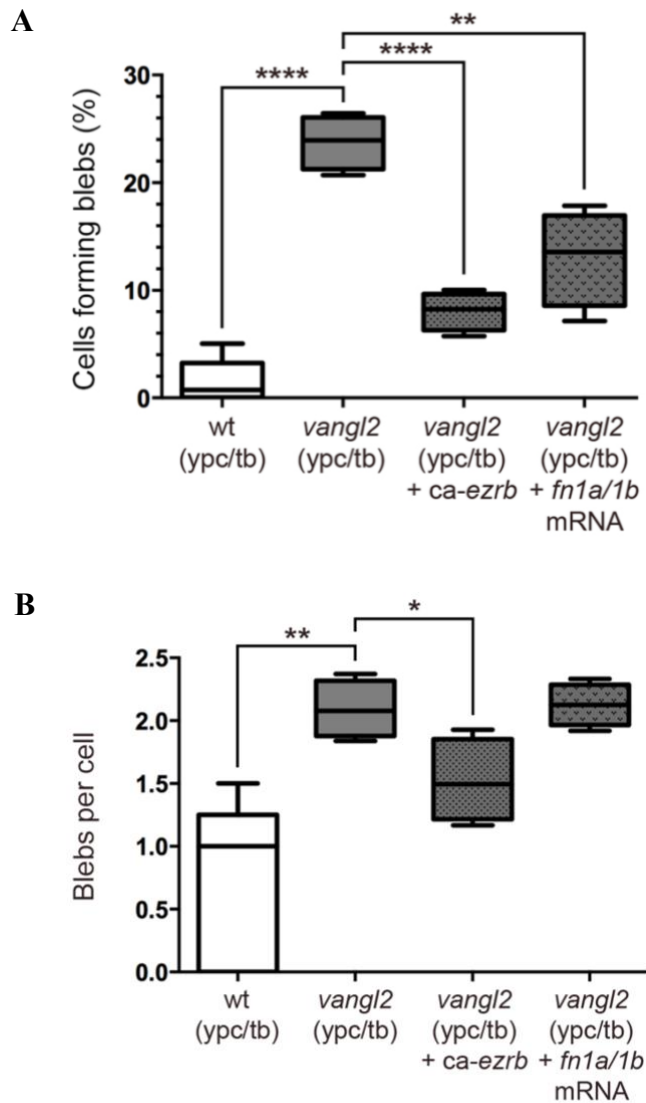


Figure 26. Loss of Vangl2 increases blebbing in mesodermal cells: (A) Percentage of mesodermal cells forming bleb protrusions in wild-type, *vangl2* mutant, and *vangl2* mutant embryos injected with *ca-ezrb* and *fn1a/1b* mRNA. Analysis is from 15-minute DIC time-lapse videos. (B) Quantification of blebs per cell in wild-type, *vangl2* mutant, and *vangl2* mutant embryos injected with *ca-ezrb* and *fn1a/1b* mRNA. Box plots display data as the interquartile range, the median and data range (*vangl2*^{*vu67/vu67*}, n=560 cells, 4 embryos, *vangl2*^{*vu67/vu67*}+*ca-ezrb*, n=560 cells, 4 embryos; *vangl2*^{*vu67/vu67*}+*fn1a/1b* mRNA, n=560 cells, 4 embryos). * $P < 0.05$, ** $P < 0.01$, **** $P < 0.0001$; unpaired Student's *t*-test with Welch's correction. Ypc/tb, yolk-plug closure/tailbud stage.

To analyze the effects on directed migration, individual mesodermal cell tracking was performed using FIJI software, and directness was calculated in reference to the dorsal axis. Compared to wild-type mesodermal cells (0.91), *vangl2* mutant mesodermal cells displayed decreased migration directness (0.53). When *vangl2* mutant embryos are injected with either *ca-ezrb* or *fn1a/1b* mRNA, migration directness was significantly increased (*vangl2^{vu67/vu67}+ca-ezrb* mRNA=0.71, *vangl2^{vu67/vu67}+fn1a/1b* mRNA = 0.73 (Figure 27A,B)).

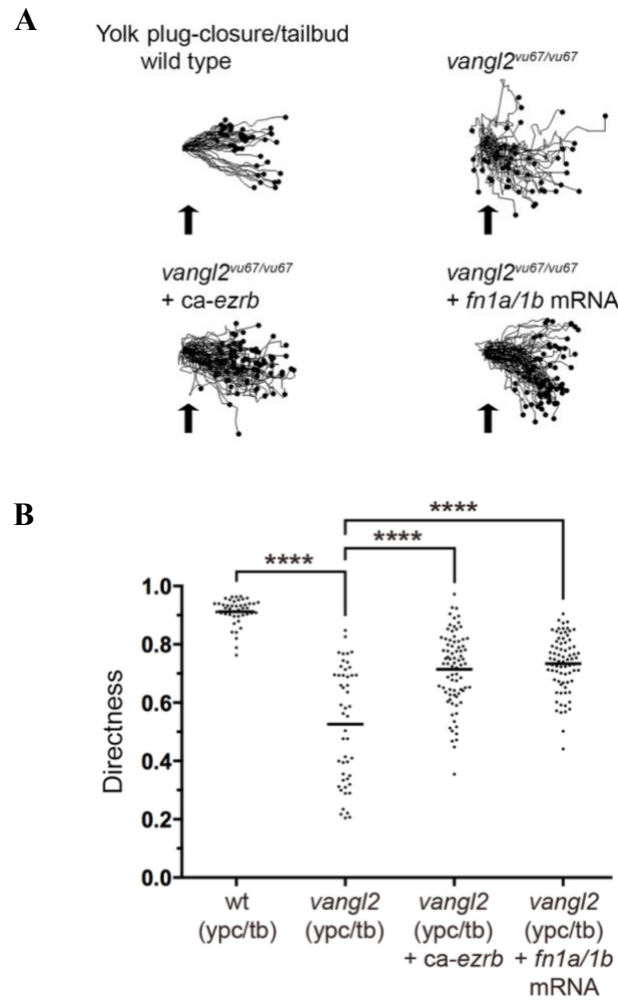


Figure 27. Inhibition of blebbing in *vangl2* mutants increases directed migration: (A) Individual cell migration tracks showing dorsal convergence of mesodermal wild-type, *vangl2* mutant, and *vangl2* mutant embryos injected with *ca-ezrb* and *fn1a/1b* mRNA. Black arrows show standard point of origin for comparison. **(B)** Individual mesodermal cell directness values (*vangl2^{vu67/vu67}*, n=50 cells, 3 embryos; *vangl2^{vu67/vu67}*+ *ca-ezrb*, n=80 cells, 3 embryos; *vangl2^{vu67/vu67}*+ *fn1a/1b* mRNA, n=75 cells, 3 embryos). Scatter plot shows individual data points and average values. **** $P < 0.0001$; unpaired Student's *t*-test with Welch's correction. Ypc/tb, yolk-plug closure/tailbud stage.

***vangl2* acts cell-autonomously to regulate bleb protrusions, and loss of fibronectin non-autonomously disrupts protrusion formation and polarity**

To determine how Vangl2 regulates cell blebbing and filopodia, a series of cell transplantation experiments and fluorescent confocal time-lapse imaging was performed. Donor embryos were injected with a combination of Lifeact-GFP, memRFP, and for some experiments, a *vangl2* MO (Figure 28A). For the first transplantation scheme, wild-type control donor embryos were injected with Lifeact-GFP and host embryos were non-injected. These transplanted mesodermal cells had an LWR of 1.71 and $MLA \pm 20^\circ = 70\%$ and served as our control. The number of cells forming blebs was 0/10 with a total of 0 blebs formed. In the next transplantation scheme, wild-type donor embryos were injected with a *vangl2* MO and Lifeact-GFP then transplanted into non-injected wild-type host embryos. We observed an LWR of 1.29, $MLA \pm 20^\circ = 18\%$, and the number of cells forming blebs was 6/8 with 24 total blebs being formed.

Next, the opposite experiment was performed. Wild-type donor embryos were injected with Lifeact-GFP and transplanted into wild-type host embryos injected with *vangl2* MO. The LWR was 1.29 and $MLA \pm 20^\circ = 27\%$. The number of cells forming blebs was 0/16 with 0 total blebs being formed. For comparison, fibronectin was also tested. Donor embryos were injected with Lifeact-GFP then transplanted into wild-type hosts injected with *fn1a/1b* MO's (Figure 28B). These cells had an LWR of 1.40, $MLA \pm 20^\circ = 31\%$, and the number of cells forming blebs was 2/14 with 10 blebs formed total (Figure 28C).

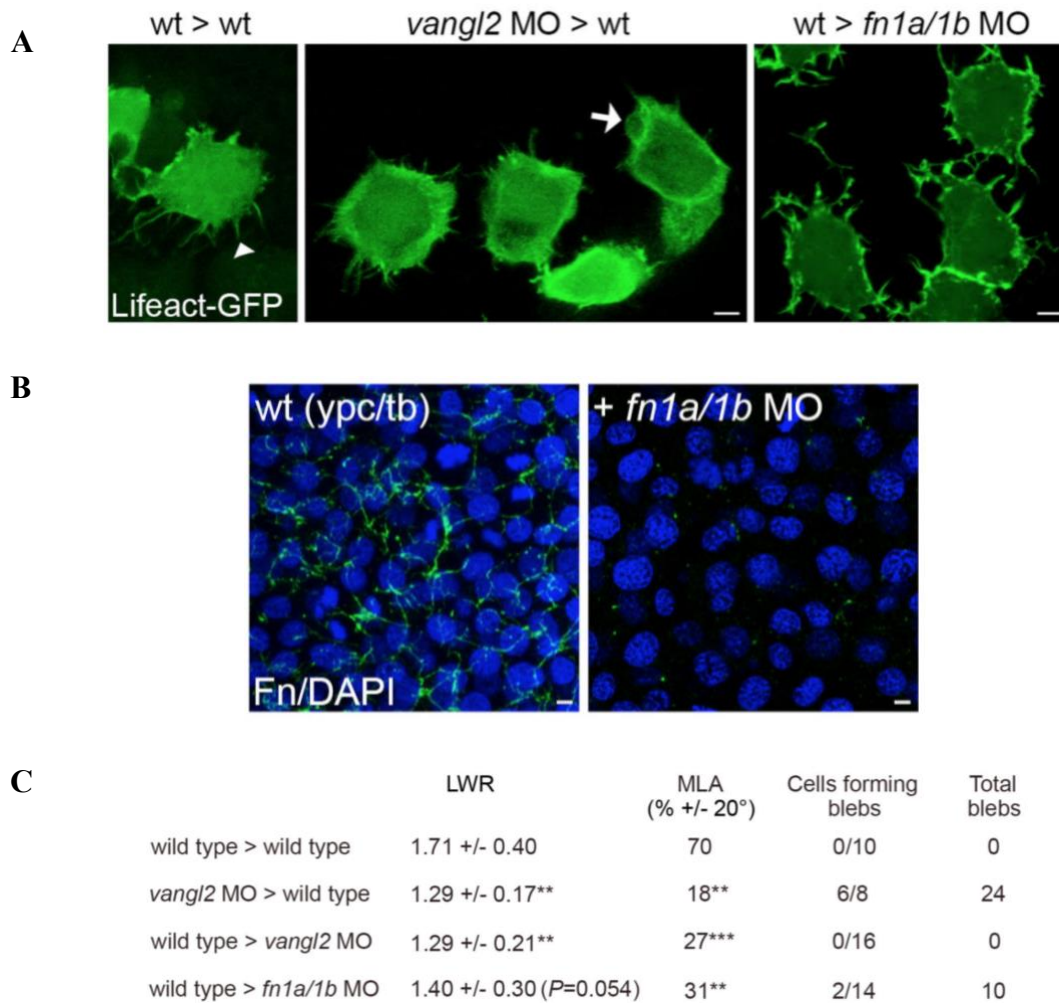


Figure 28. *vangl2* acts cell-autonomously to regulate bleb protrusions: (A) Donor cells labeled with Lifeact-GFP (green) transplanted into host embryos. White arrowhead denotes filopodia protrusion and white arrow denotes a bleb protrusion. (B) Fibronectin (green)/DAPI (blue) immunolabeling in wild-type control and wild-type embryos injected with *fn1a/1b* MO. (C) Quantification of PCP (LWR and MLA) and bleb protrusions in Lifeact-GFP labeled mesodermal donor cells (wild type>wild type, n=10 cells, 5 embryos; *vangl2* MO>wild type, n=8 cells, 3 embryos; wild type>*vangl2* MO, n=16 cells, 6 embryos; wild type>*fn1a/1b* MO, n=14 cells, 4 embryos). ** $P<0.01$, *** $P<0.001$; unpaired Student's *t*-test. Scale bars, 5 μ m.

***vangl2* acts cell-autonomously to regulate filopodia, and loss of fibronectin non-autonomously disrupts protrusion formation and polarity**

In addition to blebs, filopodia were counted from the same 15-minute transplantation time-lapse videos. These results showed an increase in the number of filopodia formed compared to wild-type control when *vangl2* MO injected cells were transplanted to a wild-type host, but no difference was observed when wild-type cells were transplanted to a *vangl2* MO injected host (Figure 31A). Filopodia were classified as polarized when they were $\pm 20^\circ$ of the dorsal body axis. Here, the only significant difference observed was in transplanted wild-type cells into a fibronectin knockdown environment where we see a decrease in the number of polarized filopodia compared to control transplantations (Figure 29A,B).

Overall, we found a wild-type host environment did not suppress bleb or filopodia protrusion formation in *vangl2* morphant donor cells. In contrast, we found wild-type donor cells transplanted to a *vangl2* morphant host did not exhibit abnormal protrusive activity. These data suggest *vangl2* functions cell-autonomously to regulate protrusion formation. Lastly, we found loss of fibronectin non-autonomously disrupted protrusion formation and polarity.

Vangl2 mutants have decreased total and activated Ezrinb

Because bleb protrusions were increased in *vangl2* mutant mesodermal cells, we hypothesized *vangl2* mutants could have disrupted expression or activation of Ezrb. To determine this, western blots were used to analyze total protein and phosphorylated levels of Ezrb in *vangl2* mutant and wild-type embryos. Our data show a significant decrease of

total and phosphorylated protein levels of Ezrb in *vangl2* mutant embryos compared to controls (Figure 30A,B).

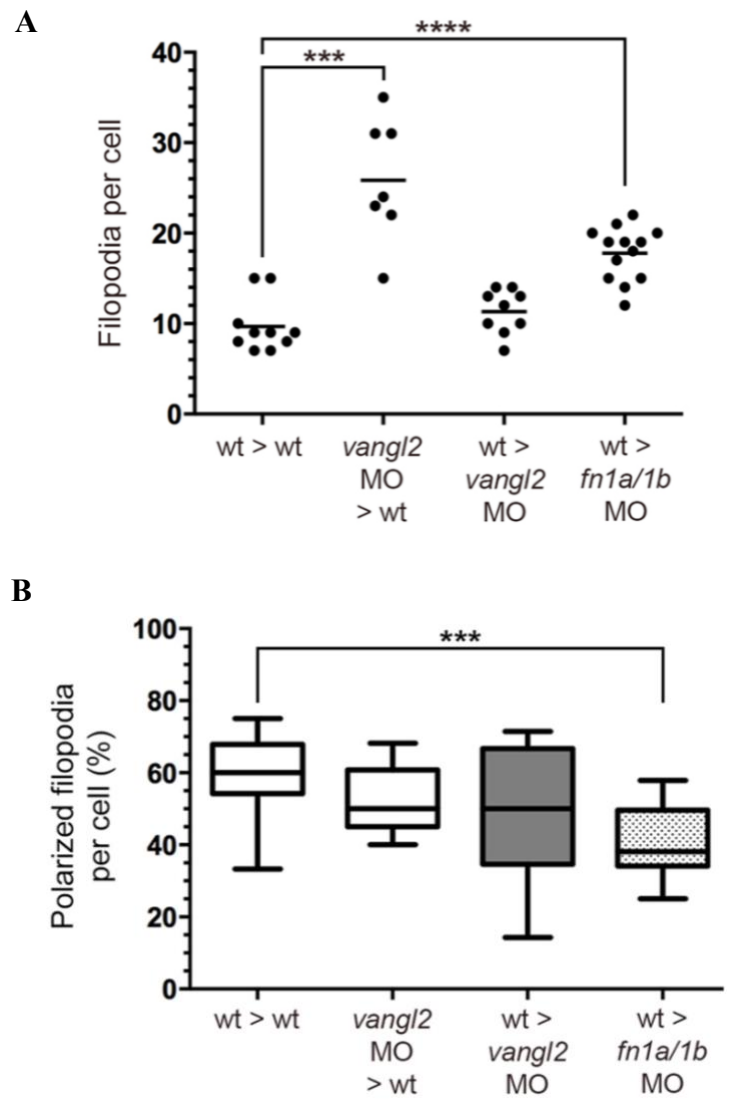


Figure 29. *vangl2* acts cell-autonomously to regulate filopodia protrusions (A) Donor filopodia quantification in transplanted mesodermal donor cells (wild type>wild type, n=10 cells, 5 embryos; *vangl2* MO>wild type, n=8 cells, 3 embryos; wild type>*vangl2* MO, n=16 cells, 6 embryos; wild type>*fn1a/1b* MO, n=14 cells, 4 embryos). **(B)** Percentage of filopodia polarized in donor cells. Scatter plot (A) shows individual data points and average values. Box plot (B) displays data as the interquartile range, the median and data range. *** $P < 0.00$, **** $P < 0.000$; unpaired Student's *t*-test with Welch's correction.

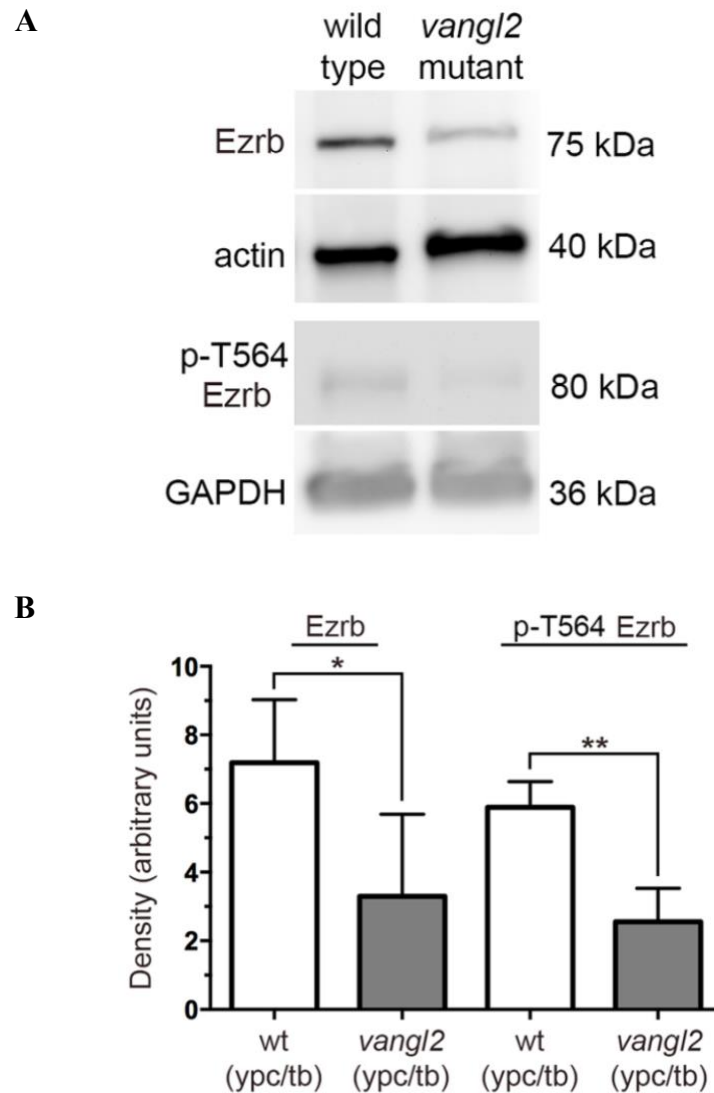


Figure 30. Ezrinb protein expression in *vangl2* mutant embryos: (A) Representative western blot of total Ezrb and phosphorylated (p-T564 Ezrb) protein levels. (B) Average band density quantified from western blots. Western blots were done in triplicate. Bar graph shows average values \pm the standard deviation. * $P < 0.05$, ** $P < 0.01$; unpaired Student's *t*-test with Welch's correction.

6.3 Conclusion

In this chapter, we aimed to establish the role of Vangl2 in bleb protrusion formation and determine if *vangl2* mutant defects are due to improper bleb protrusion regulation. We found *vangl2* mutant mesodermal cells do generate significantly more bleb protrusions than wild-type mesodermal cells suggesting Vangl2 does function during gastrulation to suppress bleb formation. Next, we found injection of *vangl2* mutants with a *ca-ezrb* mRNA significantly suppressed blebbing in mesodermal cells which resulted in a significant increase in MLA and directed migration. We suggest this is due to a switch from bleb to actin-based protrusions which inhibits tumbling phases of migration and stimulates packing. Next, injection of *vangl2* mutants with *fn1a/1b* mRNA was also sufficient to significantly suppress blebbing and partially rescue MLA and directed migration of mesodermal cells. We propose this is due to *vangl2* mutants having decreased fibronectin protein levels (Dohn et al., 2013).

Additionally, we aimed to determine how, either cell-autonomously or non-autonomously, *vangl2* regulates protrusion formation. Cell transplantation experiments revealed that *vangl2* regulates bleb and filopodia formation cell-autonomously. This means *vangl2* mutant cells do not transfer protrusion defects onto neighboring wild-type cells. For comparison, we also analyzed the effect of *fibronectin* morphant mesodermal cells had on surrounding wild-type host cells and found they non-autonomously regulated protrusion formation. Lastly, we found *vangl2* mutant embryos had significant reductions of Ezrb total and phosphorylated protein by western blot. This data suggests Vangl2 mediates the reduction in bleb protrusive activity at late gastrulation through effects on Ezrb protein expression.

CHAPTER SEVEN. Discussion

PCP is fundamental to C&E cell movements occurring during zebrafish gastrulation. Loss of PCP protein function results in embryos with a strong C&E phenotype characterized by defective elongation and MLA of gastrula cell populations (Jessen et al., 2002; Topczewski et al., 2001). At mid-gastrulation cells are undergoing PCP-independent migration as evidenced by meandering trajectories, limited cell-cell contacts, and decreased cohesion. By late gastrulation, cells exhibit PCP-dependent behaviors depicted by increased elongation and mediolateral alignment and straightened migration paths. These and other data have provided a broad functional definition for PCP proteins like Vangl2. However, it remains unclear what entails this key transitional period from PCP-independent to PCP-dependent cell migration. In this study, we aimed to detail membrane-protrusive activity during this developmental period and its regulation by Vangl2 and to determine the requirement of fibronectin and Cdh2 for PCP establishment.

We report that zebrafish mesendodermal/mesodermal cells form a combination of actin-based and bleb protrusions from mid- to late gastrulation. It has been shown certain cell types such as primordial germ cells undergo an amoeboid type of migration (Blaser et al., 2006), and early mesendodermal cells (prior to 80% epiboly) migrating anteriorly towards the animal pole use bleb protrusions during phases of reorientation (tumbling) and actin-based protrusions during active migration (runs). We now show mesendodermal cells at mid-gastrulation produce more bleb protrusions than mesodermal cells at late gastrulation. Additionally, this corresponds with an increase in filopodia from mid- to late gastrulation. This data indicates blebbing may be more productive at mid-gastrulation stages when little ECM (Latimer and Jessen, 2010), and there is decreased

cohesion/increased gaps between cells. It is known migration velocity at mid-gastrulation is higher than late gastrulation (Jessen et al., 2002). Using blebs as a major protrusion at mid-gastrulation would support a faster integrin-independent mode of migration (Charras and Sahai, 2014). This is in comparison to late gastrulation stages when a fibrillar ECM is present (Latimer and Jessen, 2010) and cells switch to a primarily actin-based protrusion mode of migration. However, our data also showed inhibition of blebbing by injection of *ca-ezrb* or *fn1a/1b* mRNA promoted directed migration. We propose this is due to a switch from blebs to actin-based protrusions (Diz-Muñoz et al., 2016), thereby preventing tumbling phases of migration and increasing packing. We propose Ezrinb protein expression is responsible for differential blebbing in mesendodermal and mesodermal cells. Indeed, we show protein levels of activated Ezrinb are increased in wild-type embryos at late gastrulation compared to mid-gastrulation.

The typical model for single cell migration suggests that pseudopodia production occurs at the leading edge of the cell while retraction occurs in the trailing edge. However, when analyzing gastrula cells undergoing collective migration we did not observe polarity in leading edge filopodia protrusions. Instead we found filopodia are mediolaterally polarized and the amount polarized filopodia increases from mid- to late gastrulation. We also found this increase in mediolaterally polarized filopodia requires Vangl2 function. Our previously published data showed ectodermal gastrula cells utilized mediolaterally polarized protrusions during directed migration also (Love et al., 2018). This data from ectoderm combined with this current data from mesoderm indicate gastrula cells migrate by using bipolar protrusions. The significance of mediolateral protrusion polarity for mesodermal and ectodermal gastrula cells is not understood. However, *Xenopus laevis*

(frog) polarized gastrula cells use medially and laterally produced protrusions during mediolateral intercalation to generate traction forces by attaching to adjacent cells or the ECM (Keller and Shook, 2008). Filopodia are recognized as functioning to probe the ECM and has the ability to express integrins and cadherins (Jacquemet et al., 2015). Therefore, mediolaterally polarized filopodia may function to sense the ECM and neighboring cells to promote elongation and MLA.

The reduction in bleb protrusions by late gastrulation suggests this type of protrusion is not preferred or is inhibitory at this stage. We found that increased blebbing in mesodermal cells after *ezrinb* MO injection did have negative impacts on PCP and directed migration.

During the transition of PCP-independent to PCP-dependent cell migration occurring between mid- to late gastrulation, a correlated increase in fibronectin ECM and cell surface expression of cadherin occurs (Latimer and Jessen, 2010). The ECM has a great impact on cell migration (Charras and Sahai, 2014) and cells respond to changes in ECM by switching between bleb and actin-based modes of migration (Tozluoğlu et al., 2013). We show manipulation of fibronectin at late gastrulation is sufficient to increase blebbing and disrupt PCP and directed migration. This suggests that a positive feedback loop exists between PCP signaling and fibronectin. The appearance of a fibrillar ECM correlates with the onset of PCP. We propose a relationship between bleb protrusion formation and the appearance of fibronectin. Our data support this showing expression of *fn1a/1b* mRNA in wild-type embryos at mid-gastrulation and *vangl2* mutant embryos at late gastrulation reduces blebbing and increases MLA.

In addition to cell-ECM interactions, cell migration involves dynamic interactions with its neighbors as cells undergo collective migration. Our data show cell surface Cdh2 expression increases from mid- to late gastrulation, and loss of Cdh2 function increases blebbing and disrupts PCP at late gastrulation. Studies during frog gastrulation show cadherin-mediated mechanotension can influence fibronectin assembly through the actin cytoskeleton. Therefore, increased blebbing in *cdh2* morphants and mutants may be due to effects on fibronectin assembly.

Mesodermal cells in *vangl2* mutant embryos lack PCP, causing cells to remain round, lack MLA, and have indirect migration trajectories. We show Vangl2 regulates bleb suppression at late gastrulation, in addition to filopodia polarity. We propose increased blebbing by *vangl2* mutant mesodermal cells is due to disrupted directed migration and MLA. When *vangl2* mutant embryos are injected with *fn1a/1b* or *ca-erzb* mRNA, blebbing was suppressed and MLA and directed migration was slightly rescued. Our data indicates proper MLA is required for successful dorsal convergence. Elongation of *vangl2* mutant mesodermal cells was not rescued further indicating elongation is regulated by other forces such as mediolaterally polarized filopodia. Other studies have shown that cell elongation and MLA occurs simultaneously (Roszko et al., 2015), but can be regulated independently of one another (Marlow et al., 2002). We also note that injection of *vangl2* mutants with *ca-ezrb* or *fn1a/1b* mRNA does not rescue the C&E phenotype. This is likely due to wild-type ectodermal cells producing few blebs, and *vangl2* mutant ectodermal cells not having increased blebbing (Love et al., 2018). Therefore, injection of *ca-ezrb* or *fn1a/1b* mRNA is unlikely to influence the *vangl2* mutant ectoderm defects.

How does Vangl2 regulate membrane protrusions? Our previous data from ectoderm show Vangl2 becomes more enriched in protrusions shortly before its collapse (Love et al., 2018). It is established that *vangl2* acts cell-autonomously and non-autonomously to control cell polarity (Jessen et al., 2002). We show by cell transplantation that *vangl2* acts cell-autonomously to regular bleb and filopodia formation. How does Vangl2 only have autonomous effects on protrusion formation? *vangl2* morphants and germline mutants, though decreased, still have a moderate level of fibronectin.

We also show *vangl2* mutants have decreased activated and total protein levels of Ezrinb. This supports our cell transplantation data indicating *vangl2* functions cell-autonomously to regulate Ezrinb expression to weaken the linkage between the membrane and cortical actin, thereby promoting blebbing. It is not known how Vangl2 could regulate Ezrinb and whether this could be a direct or indirect effect. We hypothesize Vangl2 could regulate Ezrinb expression by effects on Rho-associated coiled-coil containing protein kinase (Rock). Rock is known to activate myosin II to promote actomyosin contractility. Other studies have also implicated Rock as having the ability to activate ezrin (Matsui et al., 1998). Furthermore, in zebrafish Rock2a has been shown to regulate PCP and directed cell migration in gastrula cells. Limited data has also suggested Vangl2 functions to stabilize Rock2a at the membrane (Jessen et al., 2002; Marlow et al., 2002). By increasing Ezrinb protein levels Vangl2 could inhibit blebbing and promote PCP and directed migration at late gastrulation.

Overall, this data suggests the onset of PCP requires a transition in membrane-protrusive activity. This transition is dependent on Vangl2, fibronectin, and Cdh2 function. At mid-gastrulation when little ECM is present, mesendodermal cells exhibit little cohesion

and produce more bleb protrusions. Blebbing seems to be more effective at this stage by providing fast migration (runs) and reorientation phases (tumbles). At late gastrulation when a fibrillar ECM is present, cells are more cohesive and produce actin-based protrusions that enable engagement in directed migration toward the dorsal axis. We propose Vangl2 dependent formation and polarization of filopodia facilitates PCP establishment and increased cell cohesion. In addition, we propose Vangl2 increases Ezrin levels to inhibit blebbing and promote PCP and directed migration.

We alternatively propose Vangl2 controls the proper balance of membrane-protrusive activity by regulation of actomyosin contractility in mesodermal gastrula cells. Our data is suggestive that Vangl2 mediates the change in membrane-protrusive activity from mid- to late gastrulation in addition to the change in cell morphology and directed migration. Studies have shown that changes in actomyosin contractility and cell-ECM adhesion can influence changes in modes of migration. Therefore, we hypothesize defects in *vangl2* mutant mesodermal cells is a result of altered mechanotension due to defective actomyosin contractility and cell-ECM adhesion.

Many studies have connected Vangl2 to proteins regulating transmission and generation of mechanical force such as Rho associated coiled-coil containing protein kinase 2 (Rock2), myosin light chain phosphatase (Ppp1r12a/Mypt1), and non-muscle myosin II (McGreevy et al., 2015; Ossipova et al., 2014, 2015). It is important to note that Rock2a and Ppp1r12a/Mypt1 are shown to be required for C&E cell movements and that Vangl2 can regulate the subcellular location of Rock2a in zebrafish (Jessen et al., 2002; Marlow et al., 2002; Weiser et al., 2009). Based on our data, increased blebbing in *vangl2* mutant mesodermal cells suggests increased actomyosin contractility. Therefore, we

hypothesize an increase in non-muscle myosin II activity in *vangl2* mutant mesodermal cells causes increased blebbing and consequently loss of cohesion and PCP. Further studies are needed to investigate these hypotheses.

CHAPTER EIGHT. Materials and Methods

8.1 Zebrafish Husbandry and Genetic Strains

Wild-type (AB, TL, and WIK), *vangl2^{vu67/+}*, and *cdh2^{tm101/+}* adult zebrafish (*Danio rerio*) were used in this study. Adult zebrafish were maintained using standard procedures (Solnica-Krezel et al., 1994). Embryos were collected after natural spawnings and grown at 28.5°C in egg water (60 mg/L Instant Ocean in reverse osmosis water) until desired stage (Kimmel et al., 1995). The *vangl2^{vu67}* (Solnica-Krezel et al., 1996) and *cdh2^{tm101}* alleles perform as a null mutation (loss-of-function) due to the introduction of a stop codon early in the coding sequence. The Middle Tennessee State University Institutional Animal Care and Use Committee (IACUC) approved this research and all procedures were conducted using approved guidelines (Office of Laboratory Animal Welfare assurance number, A4701-01).

8.2 Embryo Microinjection, Morpholinos, and Synthetic mRNA

Microinjection of embryos was performed at either one-cell-stage for overall expression or 16-cell-stage for mosaic expression experiments. Antisense morpholino oligonucleotides were obtained from Gene Tools and diluted in distilled water at a concentration of 15 µg/µL. The following previously published morpholinos were used in this study: *fn1a* (5'-tttttcacaggtgcgattgaacac-3'), *fn1b* (5'-tactgactcacgggtcattttcacc-3') and (5'-gcttctgctttgactgtatttcgg-3'), *cdh2* (5'-tctgtataaagaaaccgatagagtt-3'), *ezrb* (5'-

gatgtagatgccgattcctcctcgtc-3') and *vangl2* (5'-agttccaccttactcctgagagaat-3') (Dohn et al., 2013; Jülich et al., 2005; Latimer and Jessen, 2010; Lele et al., 2002; Link et al., 2006; Love et al., 2018). Morpholino doses were 5ng of morpholino per embryo. The morpholinos used in this study did not produce evident p53-mediated cell death. Because *ezrb* and *cdh2* were new morpholino tools in our lab, western blots were performed on whole protein extracts from *ezrb* and *cdh2* morpholino injected embryos.

Synthetic mRNA constructs used in this study consist of: Lifeact-GFP, memRFP, *ca-ezrb*, *fn1a* and *fn1b*. Synthetic mRNA transcripts were prepared using a Sp6 mMessage mMachine kit (Ambion). Linearized DNA generated from restriction enzyme-cut plasmids were purified by phenol/chloroform extraction followed by ethanol precipitation and purification with G-50 sephadex columns (Roche) to generate mRNA constructs. Due to the length of the *fn1a* and *fn1b* transcripts, 1 μ L of 20 μ M GTP was added to the transcription reaction as suggested by the manufacturer. All synthetic mRNA's were injected at approximately 150 pg/embryo.

8.3 Whole-Mount *In Situ* Hybridization

For whole-mount *in situ* hybridization, embryos were staged and fixed at 4°C with 4% paraformaldehyde diluted in PBS. After fixation, embryos were washed with PBS/T (PBS + 0.1% Tween-20) and stored in methanol before high resolution *in situ* hybridization was performed (Thisse and Thisse, 2008). First, embryos were slowly rehydrated into PBS/T and then incubated in a pre-hybridization (HYB) solution (50% formamide, 5x saline-sodium citrate (SSC), 50 μ g/ml heparin 5 mg/ml, 500 μ g/ml tRNA 50 mg/ml, 0.1% Tween 20 20%, pH 6 acide citrique 1M) for 2h at 65°C. Next, a hybridization incubation is performed overnight at 65°C with fresh pre-HYB solution and 30 – 100 ng of probe. Then,

embryos are washed with a series of HYB/SSC solutions and then SSC/PBT solutions until the embryos are in a solution of 100% PBS/T, and incubated overnight with a anti-digoxigenin antibody. Lastly, embryos are washed 6x 15 min with 100% PBS/T and 3x 5 min with alkaline Tris buffer (100mM Tris HCl pH 9.5 1M, 50mM MgCl₂ 1M, 100mM NaCl 5M, 0.1% Tween 20 20%). To stain, embryos are incubated in 700 μ L labeling mix (225 μ L NBT, 50 mL alkaline Tris buffer, 175 μ L BCIP) until desired darkness. In this study, an antisense RNA probe that recognized *protocadherin 8* was used for our experiments and made using *in vitro* transcription and purified following standard methods (Love et al., 2018; Yamamoto et al., 1998). Embryos were then imaged using an Olympus SZ51/SZ61 stereomicroscope.

8.4 Western Blotting

For western blotting, embryo whole-cell lysates were prepared using approximately 50-100 embryos. Embryos were manually dechorionated, deyolked, and lysed in RIPA buffer (50mM Tris, pH 7.4, 150mM NaCl, 1% NP-40, 0.5% DOC, 0.1% SDS, mammalian protease inhibitor cocktail). After clarification by centrifugation, Laemmli buffer (1x final concentration) was added to the whole cell lysates and boiled for 10 minutes at 95°C. Protein extracts were then separated by SDS-PAGE and transferred to a PVDF membrane using a trans-blot turbo transfer system (Bio-Rad). Membranes were blocked for 2 hours at room temperature with 2-5% non-fat milk to prevent non-specific binding and incubated overnight at 4°C with a primary antibody diluted in fresh 2-5% nonfat milk. The following antibodies were used in this study: ezrin (1:500, 610401, BD Transduction Laboratory), T567 phospho-ezrin (1:500, 3141, Cell Signaling Technology), and pan-cadherin (1:1,000, AB16505, Abcam). After primary antibody incubation, membranes were washed with

PBS/T (PBS + 0.1% Tween-20), incubated with a peroxidase-conjugated secondary antibody used at 1:5,000 (Jackson ImmunoResearch), and developed using Clarity ECL substrate (BioRad). Western blot band density was quantified with UVP VisionWorks software. As a control, membranes were then striped at room temperature for 10 minutes using 25 mM glycine and 1% SDS (pH 2.0) and re-probed with β -actin (1:1,000, 4967, Cell Signaling Technology) or GAPDH (1:1,000, AM4300, Ambion). Visualization was performed as above.

8.5 Immunofluorescence

For immunofluorescence, embryos were staged and fixed with Prefer fixative (Anatech Ltd.) for 2 hours at room temperature. Antibodies used for immunofluorescence included: pan-cadherin (1:100, AB16505, Abcam) and fibronectin (1:100, F3648, Millipore-Sigma). After fixation, embryos were manually dechorionated and permeabilized in either 100% acetone at -20°C (fibronectin) or a 5% BSA, 1% DMSO, 0.1% Triton, PBS solution for 30 minutes at room temperature (pan-cadherin). Embryos were washed with PBST-D (0.1% Triton, 1% DMSO, PBS) at room temperature and incubated with a fluorophore-conjugated secondary antibody (1:500, Jackson ImmunoResearch). For nuclei labeling, embryos were washed with PBS then incubated 30 min with DAPI (2-(4-amidinophenyl)-1H-indole-6-carboxamide) at room temperature.

8.6 DIC and Confocal Imaging

Live and fixed embryos were mounted in 0.8% low-melt agarose on coverslip dishes (In Vitro Scientific #1.5 Glass Bottom). Confocal time-lapse images were collected at 1 minute intervals for 15 minutes with a 0.5 μ m z-axis step size and was done using an inverted

Zeiss Axio Observer LSM700 laser-scanning confocal microscope with a 63x oil-immersion objective (N.A. 1.4). DIC time-lapse images were collected every 30 seconds for 15 minutes and was performed with an inverted Olympus IX83 microscope equipped with a 40x air-objective (N.A. 0.95) and a Hamamatsu Flash 4.0 CMOS camera. A Coded Intermediate MAG changer (IX3-CAS) at 1.6x was used for DIC time-lapse imaging to increase visualization of bleb protrusions. For both confocal and DIC imaging, whole-mount embryo reference images were taken by low-magnification (10x) transmitted light for confirmation of orientation.

8.7 Quantitation of PCP, Directed Migration, and Membrane Protrusions

PCP measurements (LWR and MLA) were quantified from DIC and confocal time-lapse images using Fiji software (fiji.sc) (Schindelin et al., 2012). To obtain LWR and MLA data, cells were oriented with dorsal to the right and anterior to the top. Cells were traced and LWR values were calculated by dividing the cellular length by width. Higher LWR (e.g. 2.0) indicate elongated cells with lower LWR (e.g. 1.0) values indicating more round cells. MLA values were calculated by measuring the angle between the longest point of the cell in relation to the dorsal axis and was considered mediolaterally aligned if $\pm 20^\circ$ of dorsal body axis. Cell migration directionality data was obtained by tracking individual cell movements from time-lapse videos using Fiji's Manual Cell Tracking tool. This data was transferred to Ibidi's Chemotaxis and Migration Tool standalone software (ibidi.com) to generate directness statistics and cell tracking diagrams. Directness values indicate how straight a cells path is from start point to end point and is calculated by dividing the Euclidean by accumulated distance.

To analyze membrane protrusions using confocal microscopy, a single blastomere at 16-cell-stage was injected with a mixture of Lifeact-GFP and memRFP to achieve mosaic expression. Fluorescent time-lapse images were collected for 15 minutes with 1 minute intervals. Protrusions were identified as filopodia or larger actin-based protrusions as previously described (Love et al., 2018).

DIC time-lapse imaging of bleb protrusions was similarly performed. Mesendodermal cells were classified as being in phases of “runs” or “tumbles” with parameters previously established (Diz-Munoz et al., 2016). Cells in the “run” phase were actively migrating during multiple imaging frames, while cells in the “tumble” phase were more stationary for multiple imaging frames. The polarity of actin-based and bleb protrusions was analyzed using Fiji’s Angle tool with a line drawn through the bleb and parallel to the path of migration. Mesodermal cell protrusion polarity was determined in relation to the dorsal embryonic body axis. Mesendodermal cell bleb protrusion polarity during runs and tumbles was quantified in relation to the path of movement. Protrusions formed at angles $\pm 45^\circ$ were considered polarized.

8.8 Cell Transplantation

Transplantation of cells between donor and host embryos was achieved following standard methods (Jessen et al., 2002; Roszko et al., 2015). Donor embryos were injected at the one-cell-stage with *vangl2* morpholino and/or Lifeact-GFP and memRFP. Host embryos were either not injected or injected at the one cell-stage with *vangl2* or *fn1a/1b* morpholinos. Donor embryos were allowed to develop at 28.5°C until sphere stage. Approximately 50-100 donor cells were transplanted into the margin of host embryos at 50% epiboly using an IM-11-2 pneumatic microinjector (Narishige) and 1 mm capillary needles without

filament (TW100-4, World Precision Instruments). Confocal time-lapse imaging of lateral mesodermal donor cells was performed at the *ypc/tb* stage as described above.

8.9 Statistics

Data were assembled in Microsoft Excel and exported to Prism8 (GraphPad) for graphing and statistical analyses. For these studies, we used Student's *t*-test with or without Welch's correction and Watson non-parametric two-sample U_2 test (Zar, 2009). The type of statistical test performed and the resulting significance values are noted in the figure legends as well as the numbers of cells and embryos analyzed for each experiment. The data presented have a normal distribution.

CHAPTER NINE. Bibliography

Abercrombie, M., Joan, E., Heaysman, M., and Pegrum, S.M. (1970). The locomotion of fibroblasts in culture: II. "Ruffling." *Experimental Cell Research* *60*, 437–444.

Blaser, H., Reichman-Fried, M., Castanon, I., Dumstrei, K., Marlow, F.L., Kawakami, K., Solnica-Krezel, L., Heisenberg, C.-P., and Raz, E. (2006). Migration of Zebrafish Primordial Germ Cells: A Role for Myosin Contraction and Cytoplasmic Flow. *Developmental Cell* *11*, 613–627.

Bretscher, A., Reczek, D., and Berryman, M. (1997). Ezrin: a protein requiring conformational activation to link microfilaments to the plasma membrane in the assembly of cell surface structures. *J. Cell. Sci.* *110 (Pt 24)*, 3011–3018.

Bruce, A.E.E. (2016). Zebrafish epiboly: Spreading thin over the yolk. *Developmental Dynamics* *245*, 244–258.

Carmany-Rampey, A., and Schier, A.F. (2001). Single-cell internalization during zebrafish gastrulation. *Curr. Biol.* *11*, 1261–1265.

Charras, G., and Sahai, E. (2014). Physical influences of the extracellular environment on cell migration. *Nat. Rev. Mol. Cell Biol.* *15*, 813–824.

Coleman, M.L., Sahai, E.A., Yeo, M., Bosch, M., Dewar, A., and Olson, M.F. (2001). Membrane blebbing during apoptosis results from caspase-mediated activation of ROCK I. *Nat. Cell Biol.* *3*, 339–345.

- Corda, G., and Sala, A. (2017). Non-canonical WNT/PCP signalling in cancer: Fzd6 takes centre stage. *Oncogenesis* 6, e364.
- Devenport, D. (2014). The cell biology of planar cell polarity. *J Cell Biol* 207, 171–179.
- Diz-Muñoz, A., Krieg, M., Bergert, M., Ibarlucea-Benitez, I., Muller, D.J., Paluch, E., and Heisenberg, C.-P. (2010). Control of Directed Cell Migration In Vivo by Membrane-to-Cortex Attachment. *PLoS Biol* 8.
- Diz-Muñoz, A., Romanczuk, P., Yu, W., Bergert, M., Ivanovitch, K., Salbreux, G., Heisenberg, C.-P., and Paluch, E.K. (2016). Steering cell migration by alternating blebs and actin-rich protrusions. *BMC Biol* 14.
- Dohn, M.R., Mundell, N.A., Sawyer, L.M., Dunlap, J.A., and Jessen, J.R. (2013). Planar cell polarity proteins differentially regulate extracellular matrix organization and assembly during zebrafish gastrulation. *Dev. Biol.* 383, 39–51.
- Dzamba, B.J., Jakab, K.R., Marsden, M., Schwartz, M.A., and DeSimone, D.W. (2009). Cadherin adhesion, tissue tension, and noncanonical Wnt signaling regulate fibronectin matrix organization. *Dev. Cell* 16, 421–432.
- Fackler, O.T., and Grosse, R. (2008). Cell motility through plasma membrane blebbing. *J Cell Biol* 181, 879–884.
- Friedl, P. (2004). Prespecification and plasticity: shifting mechanisms of cell migration. *Current Opinion in Cell Biology* 16, 14–23.
- Friedl, P., and Gilmour, D. (2009). Collective cell migration in morphogenesis, regeneration and cancer. *Nat. Rev. Mol. Cell Biol.* 10, 445–457.
- Gadea, G., de Toledo, M., Anguille, C., and Roux, P. (2007). Loss of p53 promotes RhoA-ROCK-dependent cell migration and invasion in 3D matrices. *J. Cell Biol.* 178, 23–30.
- George, E.L., Georges-Labouesse, E.N., Patel-King, R.S., Rayburn, H., and Hynes, R.O. (1993). Defects in mesoderm, neural tube and vascular development in mouse embryos lacking fibronectin. *Development* 119, 1079–1091.
- Goodrich, L.V., and Strutt, D. (2011). Principles of planar polarity in animal development. *Development* 138, 1877–1892.
- Habas, R., Kato, Y., and He, X. (2001). Wnt/Frizzled Activation of Rho Regulates Vertebrate Gastrulation and Requires a Novel Formin Homology Protein Daam1. *Cell* 107, 843–854.
- Harland, R.M., and Gerhart, J. (1997). Formation and function of Spemann’s organizer. *Annual Review of Cell and Developmental Biology* 13, 611–667.

- Harrington, M.J., Hong, E., Fasanmi, O., and Brewster, R. (2007). Cadherin-mediated adhesion regulates posterior body formation. *BMC Dev. Biol.* 7, 130.
- Hayes, M.N., McCarthy, K., Jin, A., Oliveira, M.L., Iyer, S., Garcia, S.P., Sindiri, S., Gryder, B., Motala, Z., Nielsen, G.P., et al. (2018). Vangl2/RhoA Signaling Pathway Regulates Stem Cell Self-Renewal Programs and Growth in Rhabdomyosarcoma. *Cell Stem Cell* 22, 414-427.e6.
- Ho, R.K., and Kane, D.A. (1990). Cell-autonomous action of zebrafish *spt-1* mutation in specific mesodermal precursors. *Nature* 348, 728–730.
- Holtfreter, J. (1943). A study of the mechanics of gastrulation. Part I. *Journal of Experimental Zoology* 94, 261–318.
- Ikenouchi, J., and Aoki, K. (2016). Membrane bleb: A seesaw game of two small GTPases. *Small GTPases* 8, 85–89.
- Jacquemet, G., Hamidi, H., and Ivaska, J. (2015). Filopodia in cell adhesion, 3D migration and cancer cell invasion. *Curr. Opin. Cell Biol.* 36, 23–31.
- Jayasundar, J.J., Ju, J.H., He, L., Liu, D., Meilleur, F., Zhao, J., Callaway, D.J.E., and Bu, Z. (2012). Open conformation of ezrin bound to phosphatidylinositol 4,5-bisphosphate and to F-actin revealed by neutron scattering. *J. Biol. Chem.* 287, 37119–37133.
- Jessen, J.R. (2015). Recent advances in the study of zebrafish extracellular matrix proteins. *Dev. Biol.* 401, 110–121.
- Jessen, J.R., Topczewski, J., Bingham, S., Sepich, D.S., Marlow, F., Chandrasekhar, A., and Solnica-Krezel, L. (2002). Zebrafish trilobite identifies new roles for *Strabismus* in gastrulation and neuronal movements. *Nat. Cell Biol.* 4, 610–615.
- Jülich, D., Geisler, R., Holley, S.A., and Tübingen 2000 Screen Consortium (2005). Integrin α 5 and delta/notch signaling have complementary spatiotemporal requirements during zebrafish somitogenesis. *Dev. Cell* 8, 575–586.
- Kane, D.A., Hammerschmidt, M., Mullins, M.C., Maischein, H.M., Brand, M., van Eeden, F.J., Furutani-Seiki, M., Granato, M., Haffter, P., Heisenberg, C.P., et al. (1996). The zebrafish epiboly mutants. *Development* 123, 47–55.
- Kane, D.A., McFarland, K.N., and Warga, R.M. (2005). Mutations in half baked/E-cadherin block cell behaviors that are necessary for teleost epiboly. *Development* 132, 1105–1116.
- Keller, R., and Shook, D. (2008). Dynamic determinations: patterning the cell behaviours that close the amphibian blastopore. *Philos Trans R Soc Lond B Biol Sci* 363, 1317–1332.

- Kibar, Z., Vogan, K.J., Groulx, N., Justice, M.J., Underhill, D.A., and Gros, P. (2001). *Ltap*, a mammalian homolog of *Drosophila Strabismus/Van Gogh*, is altered in the mouse neural tube mutant *Loop-tail*. *Nat Genet* 28, 251–255.
- Kurayoshi, M., Oue, N., Yamamoto, H., Kishida, M., Inoue, A., Asahara, T., Yasui, W., and Kikuchi, A. (2006). Expression of *Wnt-5a* is correlated with aggressiveness of gastric cancer by stimulating cell migration and invasion. *Cancer Res.* 66, 10439–10448.
- Latimer, A., and Jessen, J.R. (2010). Extracellular matrix assembly and organization during zebrafish gastrulation. *Matrix Biology* 29, 89–96.
- Lei, Y.-P., Zhang, T., Li, H., Wu, B.-L., Jin, L., and Wang, H.-Y. (2010). *VANGL2* mutations in human cranial neural-tube defects. *N. Engl. J. Med.* 362, 2232–2235.
- Lele, Z., Folchert, A., Concha, M., Rauch, G.-J., Geisler, R., Rosa, F., Wilson, S.W., Hammerschmidt, M., and Bally-Cuif, L. (2002). *parachute/n-cadherin* is required for morphogenesis and maintained integrity of the zebrafish neural tube. *Development* 129, 3281–3294.
- Link, V., Carvalho, L., Castanon, I., Stockinger, P., Shevchenko, A., and Heisenberg, C.-P. (2006). Identification of regulators of germ layer morphogenesis using proteomics in zebrafish. *J. Cell. Sci.* 119, 2073–2083.
- Love, A.M., Prince, D.J., and Jessen, J.R. (2018). *Vangl2*-dependent regulation of membrane protrusions and directed migration requires a fibronectin extracellular matrix. *Development* 145.
- Maître, J.-L., and Heisenberg, C.-P. (2013). Three Functions of Cadherins in Cell Adhesion. *Curr Biol* 23, R626–R633.
- Marlow, F., Zwartkruis, F., Malicki, J., Neuhauss, S.C., Abbas, L., Weaver, M., Driever, W., and Solnica-Krezel, L. (1998). Functional interactions of genes mediating convergent extension, knypek and trilobite, during the partitioning of the eye primordium in zebrafish. *Dev. Biol.* 203, 382–399.
- Marlow, F., Topczewski, J., Sepich, D., and Solnica-Krezel, L. (2002). Zebrafish Rho kinase 2 acts downstream of *Wnt11* to mediate cell polarity and effective convergence and extension movements. *Curr. Biol.* 12, 876–884.
- Matsui, T., Maeda, M., Doi, Y., Yonemura, S., Amano, M., Kaibuchi, K., Tsukita, S., and Tsukita, S. (1998). Rho-kinase phosphorylates COOH-terminal threonines of ezrin/radixin/moesin (ERM) proteins and regulates their head-to-tail association. *J. Cell Biol.* 140, 647–657.
- Mattila, P.K., and Lappalainen, P. (2008). Filopodia: molecular architecture and cellular functions. *Nature Reviews Molecular Cell Biology* 9, 446–454.

- McFarland, K.N., Warga, R.M., and Kane, D.A. (2005). Genetic locus half baked is necessary for morphogenesis of the ectoderm. *Dev. Dyn.* *233*, 390–406.
- McGreevy, E.M., Vijayraghavan, D., Davidson, L.A., and Hildebrand, J.D. (2015). Shroom3 functions downstream of planar cell polarity to regulate myosin II distribution and cellular organization during neural tube closure. *Biol Open* *4*, 186–196.
- Mejillano, M.R., Kojima, S., Applewhite, D.A., Gertler, F.B., Svitkina, T.M., and Borisy, G.G. (2004). Lamellipodial Versus Filopodial Mode of the Actin Nanomachinery: Pivotal Role of the Filament Barbed End. *Cell* *118*, 363–373.
- Mishra, A.K., Mondo, J.A., Campanale, J.P., and Montell, D.J. (2019). Coordination of protrusion dynamics within and between collectively migrating border cells by myosin II. *Mol. Biol. Cell* *30*, 2490–2502.
- Nagaoka, T., Ohashi, R., Inutsuka, A., Sakai, S., Fujisawa, N., Yokoyama, M., Huang, Y.H., Igarashi, M., and Kishi, M. (2014). The Wnt/Planar Cell Polarity Pathway Component Vangl2 Induces Synapse Formation through Direct Control of N-Cadherin. *Cell Reports* *6*, 916–927.
- Nose, A., Tsuji, K., and Takeichi, M. (1990). Localization of specificity determining sites in cadherin cell adhesion molecules. *Cell* *61*, 147–155.
- Ohkawara, B., Yamamoto, T.S., Tada, M., and Ueno, N. (2003). Role of glypican 4 in the regulation of convergent extension movements during gastrulation in *Xenopus laevis*. *Development* *130*, 2129–2138.
- Ossipova, O., Kim, K., Lake, B.B., Itoh, K., Ioannou, A., and Sokol, S.Y. (2014). Role of Rab11 in planar cell polarity and apical constriction during vertebrate neural tube closure. *Nat Commun* *5*, 3734.
- Ossipova, O., Kim, K., and Sokol, S.Y. (2015). Planar polarization of Vangl2 in the vertebrate neural plate is controlled by Wnt and Myosin II signaling. *Biol Open* *4*, 722–730.
- Paluch, E.K., and Raz, E. (2013). The role and regulation of blebs in cell migration. *Curr Opin Cell Biol* *25*, 582–590.
- Puvirajesinghe, T.M., Bertucci, F., Jain, A., Scerbo, P., Belotti, E., Audebert, S., Sebbagh, M., Lopez, M., Brech, A., Finetti, P., et al. (2016). Identification of p62/SQSTM1 as a component of non-canonical Wnt VANGL2-JNK signalling in breast cancer. *Nat Commun* *7*, 10318.
- Roszko, I., S. Sepich, D., Jessen, J.R., Chandrasekhar, A., and Solnica-Krezel, L. (2015). A dynamic intracellular distribution of Vangl2 accompanies cell polarization during zebrafish gastrulation. *Development* *142*, 2508–2520.

- Rottner, K., Faix, J., Bogdan, S., Linder, S., and Kerkhoff, E. (2017). Actin assembly mechanisms at a glance. *J Cell Sci* *130*, 3427–3435.
- Sahai, E. (2005). Mechanisms of cancer cell invasion. *Curr. Opin. Genet. Dev.* *15*, 87–96.
- Schlessinger, K., Hall, A., and Tolwinski, N. (2009). Wnt signaling pathways meet Rho GTPases. *Genes Dev.* *23*, 265–277.
- Schmitz, B., and Campos-Ortega, J.A. (1994). Dorso-ventral polarity of the zebrafish embryo is distinguishable prior to the onset of gastrulation. *Roux Arch. Dev. Biol.* *203*, 374–380.
- Sechler, J.L., Takada, Y., and Schwarzbauer, J.E. (1996). Altered rate of fibronectin matrix assembly by deletion of the first type III repeats. *J. Cell Biol.* *134*, 573–583.
- Sepich, D.S., Calmelet, C., Kiskowski, M., and Solnica-Krezel, L. (2005). Initiation of convergence and extension movements of lateral mesoderm during zebrafish gastrulation. *Dev. Dyn.* *234*, 279–292.
- Skoglund, P., and Keller, R. (2010). Integration of planar cell polarity and ECM signaling in elongation of the vertebrate body plan. *Curr. Opin. Cell Biol.* *22*, 589–596.
- Solnica-Krezel, L., and Driever, W. (1994). Microtubule arrays of the zebrafish yolk cell: organization and function during epiboly. *Development* *120*, 2443–2455.
- Solnica-Krezel, L., and Sepich, D.S. (2012). Gastrulation: making and shaping germ layers. *Annu. Rev. Cell Dev. Biol.* *28*, 687–717.
- Solnica-Krezel, L., Stemple, D.L., Mountcastle-Shah, E., Rangini, Z., Neuhauss, S.C., Malicki, J., Schier, A.F., Stainier, D.Y., Zwartkruis, F., Abdelilah, S., et al. (1996). Mutations affecting cell fates and cellular rearrangements during gastrulation in zebrafish. *Development* *123*, 67–80.
- Sun, L., Zou, Z., Collodi, P., Xu, F., Xu, X., and Zhao, Q. (2005). Identification and characterization of a second fibronectin gene in zebrafish. *Matrix Biol.* *24*, 69–77.
- Takeichi, M., Hatta, K., Nose, A., and Nagafuchi, A. (1988). Identification of a gene family of cadherin cell adhesion molecules. *Cell Differ. Dev.* *25 Suppl*, 91–94.
- Thisse, C., and Thisse, B. (2008). High-resolution in situ hybridization to whole-mount zebrafish embryos. *Nat Protoc* *3*, 59–69.
- Thisse, B., Heyer, V., Lux, A., Alunni, V., Degraeve, A., Seiliez, I., Kirchner, J., Parkhill, J.-P., and Thisse, C. (2004). Spatial and temporal expression of the zebrafish genome by large-scale in situ hybridization screening. *Methods Cell Biol.* *77*, 505–519.

- Topczewski, J., Sepich, D.S., Myers, D.C., Walker, C., Amores, A., Lele, Z., Hammerschmidt, M., Postlethwait, J., and Solnica-Krezel, L. (2001). The zebrafish glypican knypek controls cell polarity during gastrulation movements of convergent extension. *Dev. Cell* *1*, 251–264.
- Tozluoğlu, M., Tournier, A.L., Jenkins, R.P., Hooper, S., Bates, P.A., and Sahai, E. (2013). Matrix geometry determines optimal cancer cell migration strategy and modulates response to interventions. *Nat. Cell Biol.* *15*, 751–762.
- Wallingford, J.B., and Mitchell, B. (2011). Strange as it may seem: the many links between Wnt signaling, planar cell polarity, and cilia. *Genes Dev.* *25*, 201–213.
- Wallingford, J.B., Fraser, S.E., and Harland, R.M. (2002). Convergent extension: the molecular control of polarized cell movement during embryonic development. *Dev. Cell* *2*, 695–706.
- Warga, R.M., and Kane, D.A. (2007). A role for N-cadherin in mesodermal morphogenesis during gastrulation. *Dev. Biol.* *310*, 211–225.
- Warga, R.M., and Kimmel, C.B. (1990). Cell movements during epiboly and gastrulation in zebrafish. *Development* *108*, 569–580.
- Weeraratna, A.T., Jiang, Y., Hostetter, G., Rosenblatt, K., Duray, P., Bittner, M., and Trent, J.M. (2002). Wnt5a signaling directly affects cell motility and invasion of metastatic melanoma. *Cancer Cell* *1*, 279–288.
- Weiser, D.C., Row, R.H., and Kimelman, D. (2009). Rho-regulated myosin phosphatase establishes the level of protrusive activity required for cell movements during zebrafish gastrulation. *Development* *136*, 2375–2384.
- Wierzbicka-Patynowski, I., and Schwarzbauer, J.E. (2003). The ins and outs of fibronectin matrix assembly. *J. Cell. Sci.* *116*, 3269–3276.
- Williams, B.B., Cantrell, V.A., Mundell, N.A., Bennett, A.C., Quick, R.E., and Jessen, J.R. (2012). VANGL2 regulates membrane trafficking of MMP14 to control cell polarity and migration. *J. Cell. Sci.* *125*, 2141–2147.
- Yamamoto, A., Amacher, S.L., Kim, S.H., Geissert, D., Kimmel, C.B., and De Robertis, E.M. (1998). Zebrafish paraxial protocadherin is a downstream target of spadetail involved in morphogenesis of gastrula mesoderm. *Development* *125*, 3389–3397.
- Zhao, Q., Liu, X., and Collodi, P. (2001). Identification and characterization of a novel fibronectin in zebrafish. *Exp. Cell Res.* *268*, 211–219.